INSTITUTO DE ENGENHARIA NUCLEAR

VICTOR TAVARES CALZAVARA

STABILITY AND FLOW DISTRIBUTION ANALYSIS FOR DOWNWARD FLOW IN HEATED CHANNELS USING COMPUTATIONAL FLUID DYNAMICS MODELING

Rio de Janeiro
2019

VICTOR TAVARES CALZAVARA

STABILITY AND FLOW DISTRIBUTION ANALYSIS FOR DOWNWARD FLOW IN HEATED CHANNELS USING COMPUTATIONAL FLUID DYNAMICS MODELING

Dissertação apresentada ao Programa de Pós-graduação em Ciência e Tecnologia Nucleares do Instituto de Engenharia Nuclear como parte dos requisitos necessários para a obtenção do Grau de Mestre em Ciência e Tecnologia Nucleares

Orientadores: Maria de Lourdes Moreira
Paulo Augusto Berquó de Sampaio

Rio de Janeiro
2019

CALZ Calzavara, Victor Tavares.
STABILITY AND FLOW DISTRIBUTION ANALYSIS FOR DOWNWARD FLOW IN HEATED CHANNELS USING COMPUTATIONAL FLUID DYNAMICS MODELING / Victor Tavares Calzavara – Rio de Janeiro: CNEN/IEN, 2019.

XIV, 73 f. : il. ; 31 cm.

Orientadores: Maria de Lourdes Moreira e Paulo Augusto Berquó de Sampaio.

Dissertação (Mestrado) – Instituto de Engenharia Nuclear, PPGIEN, 2019.

1. Dinâmica dos fluidos computacional. 2. Instabilidade de escoamento. 3. Canais aquecidos. 4. Distribuição de vazão. 5. Reversão de escoamento.

STABILITY AND FLOW DISTRIBUTION ANALYSIS FOR DOWNWARD FLOW IN HEATED CHANNELS USING COMPUTATIONAL FLUID DYNAMICS MODELING

Victor Tavares Calzavara

DISSERTAÇÃO SUBMETIDA AO PROGRAMA DE PÓS-GRADUAÇÃO EM CIÊNCIA E TECNOLOGIA NUCLEARES DO INSTITUTO DE ENGENHARIA NUCLEAR DA COMISSÃO NACIONAL DE ENERGIA NUCLEAR COMO PARTE DOS REQUISITOS NECESSÁRIOS PARA A OBTENÇÃO DO GRAU DE MESTRE EM CIÊNCIA E TECNOLOGIA NUCLEARES – ÊNFASE ACADÊMICA EM ENGENHARIA DE REATORES

Aprovada por:

Prof[a]. Maria de Lourdes Moreira, D.Sc.

Prof. Paulo Augusto Berquó de Sampaio, Ph.D.

Prof. Su Jian, D.Sc.

Prof. Celso Marcelo Franklin Lapa, D.Sc.

RIO DE JANEIRO, RJ - BRASIL
AGOSTO DE 2019

Agradecimentos

Aos meus orientadores professora Maria de Lourdes Moreira e professor Paulo Augusto Berquó de Sampaio, pela sugestão de tema, orientação e conhecimentos transmitidos.

Ao engenheiro Pedro Luiz da Cruz Saldanha pelo fundamental apoio.

Aos colegas engenheiros Rafael de Oliveira Faria e Eneida Regina Guimarães Dourado Ribeiro pelo auxílio no desenvolvimento desta dissertação.

Aos meus colegas de mestrado pelo prazeroso convívio.

A todos os professores e funcionários da Pós-Graduação em Ciência e Tecnologia Nucleares do IEN.

Resumo

Modelos de Dinâmica dos Fluidos Computacional 3D são usados para analisar a distribuição de vazão e estabilidade de fluxo descendente em canais aquecidos em comparação com resultados experimentais e um modelo de escoamento unidimensional mais simples, apresentado em um trabalho anterior. O modelo 1D fornece boas previsões de distribuição de fluxo descendente entre canais, em condições de fluxo estáveis, e também uma indicação razoável do limite de estabilidade de fluxo descendente. No entanto, as previsões do modelo 1D em relação ao início da reversão de fluxo possuem limitações que foram identificadas pelo modelo CFD 3D mais detalhado apresentado. O programa ANSYS/CFX é usado nos estudos de CFD. Um conjunto completo de etapas de qualificação é realizado para garantir escolhas adequadas de malhas e modelos de fechamento de turbulência. Um experimento em uma seção de teste com dois canais paralelos, realizado em um estudo anterior, é replicado em ANSYS/CFX. Finalmente, um fluxo descendente de quatro canais é simulado em ANSYS/CFX para avaliar a precisão das previsões do modelo de fluxo 1D nessa configuração.

Palavras-chave: Dinâmica dos fluidos computacional. Instabilidade de escoamento. Canais aquecidos. Distribuição de vazão. Reversão de escoamento.

Abstract

Computational Fluid Dynamics 3D models are used to analyze stability and flow distribution of downward flow in heated channels in comparison with experimental results and with a simpler 1D flow model, presented in a previous work. The 1D model gives good predictions for the downflow distribution among channels, in stable flow conditions, and also a reasonable indication of the downflow stability limit. Nonetheless, the 1D model predictions regarding the onset of flow reversal have limitations which were identified by the more detailed CFD 3D model presented herein. The ANSYS/CFX program is used in the CFD studies. A full set of qualification steps are performed in order to ensure adequate choices of meshes and turbulence closure models. An experiment in a test section with two parallel channels, performed in a previous study, is replicated in ANSYS/CFX. Finally, a four channels downward flow is simulated in ANSYS/CFX in order to evaluate the accuracy of the 1D flow model predictions in that configuration.

Keywords: Computational fluid dynamics. Flow Instability. Heated channels. Flow distribution. Flow reversion.

List of Figures

List of Tables

List of abbreviations and acronyms

1D	One-dimensional
2D	Two-dimensional
3D	Three-dimensional
TRIGA	Training, Research, Isotopes, General Atomics (reactor)
CFD	Computational Fluid Dynamics
DNS	Direct Numerical Simulation
FCCM	Forced Convection Cooling Mode
HWLS	Hot Water Layer System
LOCA	Loss of Coolant Accident
LOECC	Loss of Emergency Core Cooling
LOFA	Loss of Flow Accident
NCCM	Natural Convection Cooling Mode
RANS	Reynolds Averaged Navier-Stokes
SCWR	Supercritical water Reactor

List of symbols

A	Flow cross-section area
C_p	Fluid specific heat capacity
D	Channel hydraulic diameter
f	Friction factor
g	Gravitational acceleration
G	Mass velocity
h	Enthalpy
h_p	Plenum height
k	Turbulent kinetic energy
K	Pressure loss coefficient
L	Channel length
P	Pressure
q''	Heat flux
Q	Heating power
$\mathbf{S}_E$	Energy source
$\mathbf{S}_M$	Momentum source
T	Temperature
$\mathbf{U}$	Velocity Vector
v	Specific volume
W	Mass flow rate

y^+	Dimensionless distance from wall
β	Volumetric coefficient of thermal expansion
ε	Turbulence dissipation rate
δ	Iterative process residual limit
λ	Thermal conductivity
μ	Viscosity
ρ	Fluid density
$\boldsymbol{\tau}$	Stress tensor
ω	Angular velocity

Subscripts

1	Channel entrance
2	Channel exit
$buoy$	Buoyant
eff	Effective
ref	Reference

Contents

1 Introduction

1.1 Pool-type Reactors Cooling Concepts

Pool-type reactors, or swimming pool reactors, are a type of nuclear reactor comprised of fuel elements and control rods assembly (core) immersed in an open pool, most commonly filled with water (SHAH, 2018). That concept is largely applied over the world in research reactors design such as TRIGA and IEA-R1.

Despite acting as a neutron moderator, the water has two major safety functions in those reactors; to be the core cooling agent and a radiation shield. During the normal operation of a pool-type water-cooled reactor, the capture of fast neutrons by O-16 present in the near-core region water produces radioactive N-16, that decays with a very high energy gamma-ray of 6.13 MeV and a short half-life of 7.14s (AJIJUL et al., 2018). That phenomenon represents a potential radiological safety issue once the water in which N-16 is present tends to flow up toward the pool surface where the reactor staff might be exposed to a significant dose amount.

Once the generation rate of the N-16 is proportional to the reactor power level, two cooling modes are possible to be used in a conventional pool-type reactor: (i) Natural Convection Cooling Mode (NCCM) and (ii) Forced Convection Cooling Mode (FCCM). At low power levels both heat removal capacity and N-16 generation technical limits can be met with the natural convection process, thus the upward flow NCCM can be used. However, when additional cooling capacity is demanded at higher power levels, the downward flow FCCM should be turned on for both cooling down the reactor core and preventing direct radiological exposure to the N-16 generated. On that mode, the primary cooling circuit piping connecting the reactor cooling pump to the bottom of the reactor core establishes a downward flow inside it and transports the in-core water to a decay tank. After the N-16 decayed to O-16, the water flows through a heat exchanger and is returned to the reactor pool, finishing its circle. A simplified flow sheet of a possible conventional pool-type reactor primary cooling circuit setup operating on forced convection mode is shown in Fig. 1.

Another engineered safety feature intended to prevent radiological exposure is called Hot Water Layer System (HWLS). That approach consists in creating a hot radioisotope-

Figure 1 – FCCM Simplifyed flowsheet

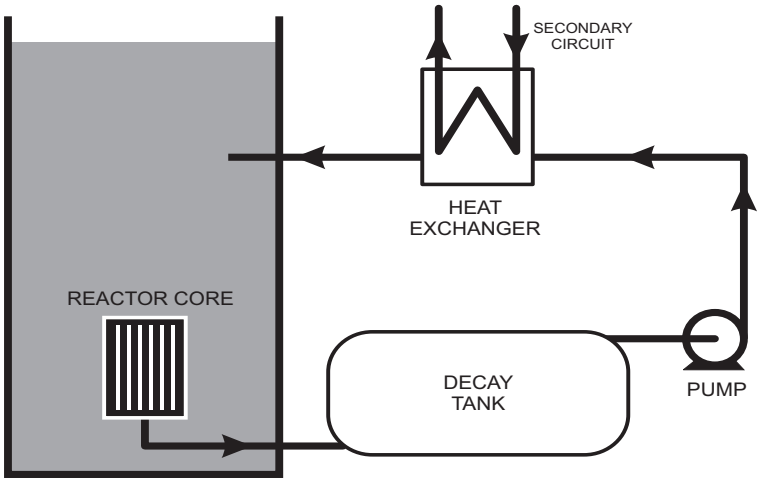

Source: Author.

free water layer at the upper portion of the pool to prevent activated products, such as the N-16, to reach its top while acting as a radiological shield, thus reducing the dose rate over the pool surface (AJIJUL et al., 2018). In contrast to the conventional way of using a downward flow cooling process associated with a decay tank to deal with N-16 issue, a pool-type reactor with a Hot Water Layer System is possible to be operated with an upward flow instead. That represents a big advantage with regards to flow stability, once the buoyant force and the reactor pump induced force have the same upward orientation.

Figure 2 – HWLS Simplifyed flowsheet (upper pool portion)

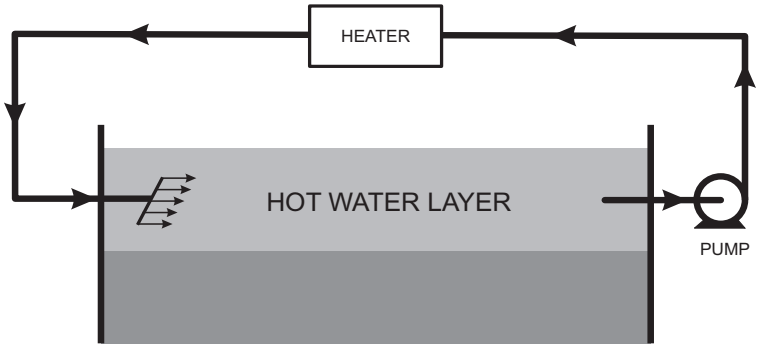

Source: Author.

1.2 Motivation

For a given combination of heat transferred to the coolant and total mass flow rate, a downward flow through the reactor core channels is expected to remain in a stable

condition. In such a case, the buoyant force induced in the coolant by the heat released from the fuel rods is overcome by the pressure difference generated by the reactor cooling pump. On the other hand, if the buoyant force is great enough to surpass that pressure difference, a reverse flow can be observed in the hot channels, as a result of the flow reaching a secondary stable condition (SAMPAIO, 1985). Fig. 3 schematically shows a reactor in-core downward flow pattern with and without a channel flow reversion. For that reason, flow stability of conventional downward flow cooled pool-type research reactors is of major importance for their design process due to potential issues that can take place during the operational phase, such as unexpected vibration and reduced core heat removal capability. In this regard, flow stability has been the subject of study in reactor conversion programs, in which the fuel type replacement (rods/plates) leads into the change of the core-cooling process from natural convection (upward flow) to forced convection (downward flow) as occurred in Bandung TRIGA Reactor (RAHARDJO; WARDHANI, 2017).

Therefore, the study of models and tools capable of predicting in-core coolant behavior regarding both flow distribution and instabilities conditions has significant importance to the safety of a nuclear installation.

Figure 3 – Left: Schematic reactor in-core downward flow pattern. Right: Schematic reactor in-core downward flow pattern with flow reversion in a hot channel.

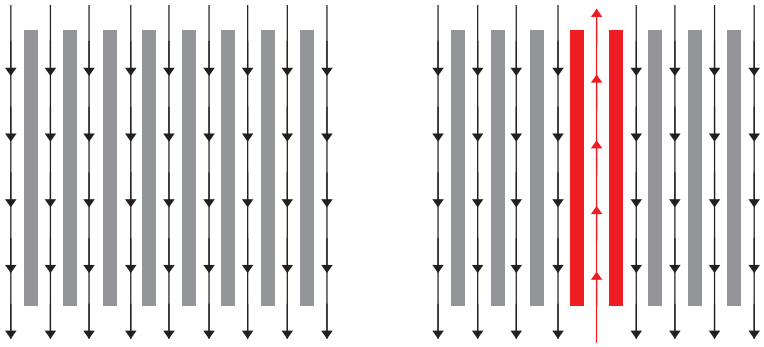

Source: Author.

1.3 Objective

Accordingly, the present work aims to compare results of flow stability and distribution obtained with Sampaio's 1D model against Computational Fluid Mechanics 3D models using Ansys CFX and thus evaluate the viability of Sampaio's 1D model to be used as a tool to predict both flow distribution and instabilities limits of pool-reactor cores.

1.4 Methodology

The methodology of this study consists of performing parallel simulations of the same given flow condition using both Sampaio's 1D model FORTRAN Program and a Ansys-CFX 3D model for further comparison of results.

For creating the Ansys-CFX 3D models, the methodology comprises the flow geometry modeling, the mesh modeling, flow conditions set up and the treatment of the resulted data.

A full set of qualification steps are done in order to assure the modeling phase described above were due performed.

Afterward, it is carried out simulation for a two and a four channels assembly. Finally, the agreement between results provided by both models are analyzed.

1.5 Organization

In chapter 2, it is presented the literature used in this work.

In chapter 3, the modeling formulations for both Sampaio's 1D model and CFX 3D model are presented.

In chapter 4, the simulations carried out are presented. That includes the qualifications phase for both mesh and turbulence models, the description and replication of Sampaio's downward flow through two channels experiment and, finally, the study of flow distribution and stability for a downward flow through four channel.

In chapter 5, results are presented and discussed.

In chapter 6, conclusions and suggestions for future works are presented.

2 Literature Review

The problem of single-phase flow instability in a poll-type reactor was observed by Boure (1961) in 1961 at the Mélusine Research Reactor. That event motivated him in a study where it was concluded that for a forced-convection cooling process, a steady-state downward flow through all the reactor core channels was impossible when the flow rate was below a critical value for a given power level.

Another relevant study regarding single-phase flow was performed by Bau and Torrance (1981) of investigation on the stability and flow reversal of an asymmetrically heated open U-shape convection loop. In that study, analytical results included a stability analysis and time-dependent one-dimensional numerical calculations, both of those well agreed with experiments. Moreover, it was observed that below a critical value of asymmetric heating, the flow oscillated with increasing amplitude until the orientation of it in the loop undergoes a reversion followed by a steady flow.

Some years later, Sampaio applied the Ledinneg criterium, typically used to evaluate two-phase flow stability, in a single-phase flow study (SAMPAIO, 1985). In his work, a simplified model intended to estimate flow distribution of a downward flow through multiple channels is introduced. Afterward, that model is used to forecast instabilities conditions and flow distribution in an experiment of downward flow through two channels undergoing different heating power using a FORTRAN program. It is worth mentioning that the unidimensional formulation Sampaio developed in that study underpins the analysis carried out in the present work. The Fig. 4 show a photograph of Sampaio's experimental framework.

Although the present work comprises the study of single-phase flow instability, the physical phenomenon characterized by the pressure drop decrease with increasing flow rate can lead both flow types to an instability condition. Accordingly, two-phase flow studies are also part of the literature bases for the present work, as follow. Boure (1973) reviewed the different types of instabilities possible to occur in a two-phase flow. Lee et al. (1977) reported experimental studies on stability for an upward flow through two parallel channels. Fukuda et al. (1984) performed a dynamic analysis for low flow rates, by using the drift-flux model. More recently, Pandey and Singh (2017) characterized the stability

Figure 4 – Sampaio's Test Section

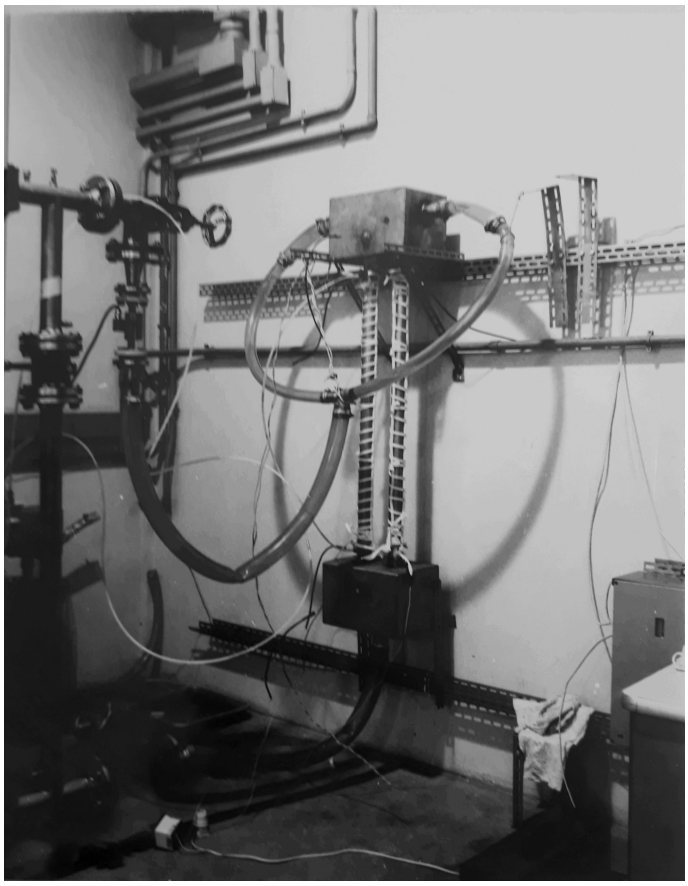

Source: (SAMPAIO, 1985)

limits of Ledinegg instability and density wave oscillation for two-phase flow in natural circulation.

Concerning computational resource applied for predicting flow behavior in the nuclear engineering field, it can be found a study performed by Smith and Woodruff (1986) where it is used a modified code to analyze the flow inversion in a reactor core with downward forced-convection heat removal mode after a pump failure with the possibility of a nucleate boiling event occurrence. In that study, it was concluded that the computer code was well suited for the proposed use.

Concerning the application of CFD, it is possible to find studies in literature well related to the scope of the present work. Among them, stands out the study carried out by Park et al. (1986) on the application of CFD on the flow stability analysis of pool-type research reactors. Park et al. (1986) simulated the flow inversion in a uniformly heated thin rectangular channel array during a LOFA (Loss of Flow Accident) where a conventional

pool-type reactor core undergoes to inversion from downward to upward flow due to the induced natural circulation. Its results were afterward compared against that one obtained from simulations with RELAP5 (one-dimensional system analysis code) and it is concluded that well detailed result, such as the fuel and coolant temperatures over time, could be provided.

Another interesting study concerns the application of CFD on flow distribution analysis, where Rebrov et al. (2011) addressed the problem of flow equalization among micro-heat-exchangers channel. In his study, it is concluded that the issue of flow equalization is usually adequately tackled by using 3D numerical models resembling the geometry of the inlet and outlet diffusers and reaction channels. Nonetheless, it is mentioned that 2D CFD models could not adequately predict flow distribution in inlet/outlet chambers and flow distribution manifolds.

Sharabi et al. (2008) applied CFD in the prediction of unstable behavior in heated channels containing supercritical fluids, in a study covering Supercritical Water Reactors (SCWRs). In that study, 2D simulations of flow passing through a heated channel connecting two rectangular plenums are carried out and their results are afterward compared against 1D computational code RELAP5. It is concluded that both the standard k–ε model with wall functions, and a more detailed low-Reynolds number model were able to predict the onset of unstable behavior in close agreement with information provided by the one-dimensional models. furthermore, it is shown that, within the limits of the analysis applicability, details in transient radial velocity distributions provided by CFD models do not significantly alter the prediction of the threshold of instability.

Kim et al. (2006) investigated the thermal-hydraulic characteristics of moderator flow subject momentum and buoyancy by heat load inside Calandria vessel of CANDU-6. In that stud, it is used the computational code 2DMOTH in simulations to predict flow behavior during normal operating condition and the transient condition of 35% reactor inlet header break loss of coolant accident (LOCA) with loss of emergency core cooling (LOECC). The simulations results were afterward compared against experimental data. It is concluded that the model could reasonably predict the temperature distributions of the moderator and had good capability to properly analyze the fluid flow subject to the buoyancy and momentum force simultaneously.

3 Modeling Formulations

3.1 Sampaio's Unidimensional Modeling Formulation

In this chapter, it is presented a theoretical review of the study developed by Sampaio (1985) to create his unidimensinal model. In his work, he analyzes the flow instability starting from the study of the pressure loss against the mass flow rate variation in a heated channel using the continuity, momentum and energy equations for a steady-state unidimensional flow through a constant cross-section area. Furthermore, Sampaio presents his model for flow distribution and flow stability in a system with multiple parallel channels.

3.1.1 Pressure Loss in a Heated Channel

Prior to the presentation of the model formulation, it is introduced the orientation conventions used by Sampaio, shown in the Fig. 5. As can be seen, a positive mass flow rate value refers to a downward flow while a negative mass flow rate value refers to an upward flow. Moreover, the channel pressure difference is defined as the entrance pressure minus the exit one, i.e., $\Delta P = P_1 - P_2$.

Figure 5 – Model Orientation Conventions

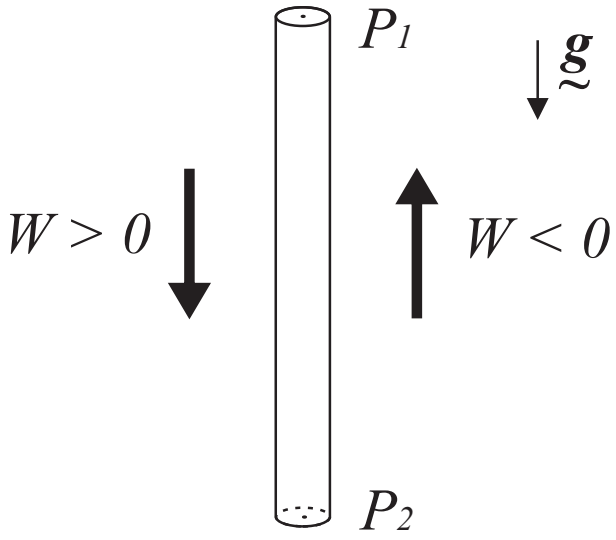

Source: Adapteded from (SAMPAIO, 1985).

Sampaio (1985) describes the pressure loss in a heated channel as follow:

$$P_2 - P_1 = \frac{-f\ G\ |G|}{2D}\ v_1\ L\left[1 + \frac{\beta\ Q}{2|G|\ A\ C_p}\right] - \frac{\beta\ Q\ v_1}{A\ C_p}\ G + \rho_1\ g\ L\ \left[1 - \frac{\beta\ Q}{2|G|\ A\ C_p}\right] \quad (3.1)$$

where:

G is the mass velocity

P is the pressure

ρ_1 is the entrance density

v_1 is the entrance specific volume

D is the hydraulic diameter

f is the friction factor

g is the gravitational acceleration

Q is the channel heating power

C_p is the fluid specific heat capacity

L is the channel length

β_1 is the volumetric coefficient of thermal expansion

Adding local pressure loss coefficients for both channel's entrance (K_1) and exit (K_2) and rearranging equation (3.1) terms, the previous equation can be written as:

$$\Delta P = a\ W|W| + b\ W + \frac{c}{|W|} - d \quad (3.2)$$

where:

$$a = \frac{v_1}{2A^2}\left[\frac{fL}{D} + K_1 + K_2\right] \quad (3.3)$$

$$b = \frac{\beta Q v_1}{A^2 C_p}\left[1 + \frac{fL}{4D} + \frac{K_1}{2}\right] \quad (3.4)$$

$$c = \frac{\rho_1\ g\ \beta Q L}{2\ C_p} \quad (3.5)$$

$$d = \rho_1 \; g \; L \tag{3.6}$$

In equation (3.1), the first term represents the pressure loss due to the flow friction for a non-heated channel. The second term represents pressure loss due to acceleration and friction, taking into consideration the heating power influence. The third term represents the pressure loss due to the gravity, related to buoyancy and, in the forth one, related to the height of fluid column.

From now on, Sampaio (1985) uses the Boussinesq approximation in his model, assuming that all fluid proprieties remain constant, but the density in the terms associated with pressure loss due to the gravity action. Thus, the second term of the equation (3.1) is neglected once $b = 0$.

Downward flow ΔP evaluation

For a downward flow ($W > 0$), the equation (3.1) becomes:

$$\Delta P = aW^2 + \frac{c}{W} - d \tag{3.7}$$

Its derivative with respect to the mass flow rate (W) is:

$$\frac{d\Delta P}{dW} = 2 \; aW - \frac{c}{W^2} \tag{3.8}$$

As shown in the equation (3.8), for a downward flow, the derivative of the pressure loss curve can became negative when the mass flow rate is reduced and the last term ($-c/W^2$) increases in modulus.

Its second derivative with respect to the mass flow rate (W) is:

$$\frac{d^2\Delta P}{dW^2} = 2 \; \left(a + \frac{c}{W^3}\right) \tag{3.9}$$

Once the equation (3.9) is positive for any value of (W), the equation (3.8) can be

used to determine the mass flow rate (W_m) where ΔP is a minimum. Thus:

$$W_m = \sqrt[3]{\frac{c}{2a}} \tag{3.10}$$

Replacing the values of "a" and "c" in the equation (3.10) as well as the energy balance defined by $Q = |G|\ A\ C_p(T_2 - T_1)$:

$$W_m = A \sqrt{\frac{\rho_1^2\ \beta\ (T_2 - T_1)\ L\ g}{2\left(\frac{fL}{D} + K_1 + K_2\right)}} \tag{3.11}$$

Upward flow ΔP evaluation

For a upward flow ($W < 0$), the equation (3.1) becomes:

$$\Delta P = -a\ |W|^2 + \frac{c}{|W|} - d \tag{3.12}$$

Its derivative with respect to the mass flow rate (W) is:

$$\frac{d\Delta P}{d|W|} = -2a\ |W| - \frac{c}{|W|^2} \tag{3.13}$$

As shown in the equation (3.13), for an upward flow, the derivative of the pressure loss curve has no point where it is equal to zero.

Its second derivative with respect to the mass flow rate (W) is:

$$\frac{d^2\Delta P}{d|W|^2} = 2\left(-a + \frac{c}{|W|^3}\right) \tag{3.14}$$

The equation (3.14) shows that for an upward flow, the pressure loss curve has an inflection point. The mass flow rate (W) where that occurs is obtained when the equation (3.14) is equal to zero, hence:

$$|W_{inflection}| = \sqrt[3]{\frac{c}{a}} \tag{3.15}$$

The Fig. (6) shows the pressure loss curve for both heated (solid line) and non-heated (dashed line) channel cases. It can be noted that for high mass flow rate absolute values, the curve for a heated channel tends to get closer to the non-heated one. Furthermore, for a downward flow, Sampaio (1985) stated that the flow is led to an instability condition when $d\Delta P/d|W|$ becomes negative due to de increased dominance of the $-c/W^2$ term in the equation (3.8) at low mass flow rate values.

Figure 6 – Pressure Loss Curve

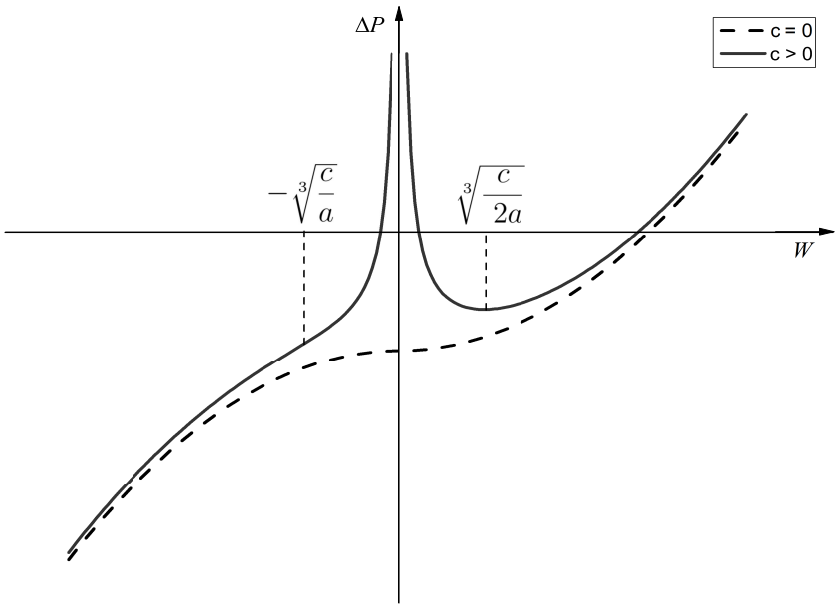

Source: Adapteded from (SAMPAIO, 1985).

3.1.2 Multiple Parallel Channels Analysis

Now it is presented the analysis performed by Sampaio (1985) for a downward flow through multiple parallel channels undergoing different heating powers. As a simplified approach, it is assumed closed channels and uniform heating power distribution.

3.1.2.1 Flow Distribution Analysis

For a given combination of total mass flow rate, geometry, and heating power, the flow distribution problem consists of determining the mass flow rate for each channel.

The pressure losses in a stead-state regime flow are the same for all the channels. Furthermore, the total mass flow rate is equal to the sum of each channel mass flow rate,

thus:

$$\left.\begin{array}{rcl} \Delta P_1 & = & \Delta P_2 \\ \Delta P_2 & = & \Delta P_3 \\ \cdot & & \cdot \\ \cdot & & \cdot \\ \cdot & & \cdot \\ \Delta P_{n-1} & = & \Delta P_n \\ \sum_{i=1}^{n} W_i & = & W \end{array}\right\} \tag{3.16}$$

Where ΔP_i is the pressure loss and W_i is the mass flow rate in the channel i. The system of equations (3.16) is non-linear with n equations and n mass flow rate values. It is solved by defining a group o F_i functions as follow:

$$F_i = \Delta P_i - \Delta P_{i+1} \; ; \; i = 1 \; , \, n-1 \tag{3.17}$$

where each F_i depends on W_i and W_{i+1}.

Expanding F_i in Taylor series around an initial guess (W_i^0,W_{i+1}^0):

$$F_i(W_i,W_{i+1}) = F_i(W_i^0,W_{i+1}^0) \; + \; (W_i - W_i^0) \left.\frac{\partial F_i}{\partial W_i}\right|_0 + \; (W_{i+1} - W_{i+1}^0) \left.\frac{\partial F_i}{\partial W_{i+1}}\right|_0 \tag{3.18}$$

Taking into consideration the definition of F_i:

$$\frac{\partial F_i}{\partial W_i} = \varepsilon_i; \; i = 1 \; , \, n-1 \tag{3.19}$$

$$\frac{\partial F_{i+1}}{\partial W_i} = -\varepsilon_{i+1}; \; i = 1 \; , \, n-1 \tag{3.20}$$

where:

$$\varepsilon_i = \frac{d\Delta P_i}{dW_i} \tag{3.21}$$

Once all the F_i are null, the system can be written in a matrix format:

$$\begin{bmatrix} \varepsilon_1^0 & -\varepsilon_2^0 & 0 & 0 & 0 \\ 0 & \varepsilon_2^0 & -\varepsilon_3^0 & 0 & 0 \\ 0 & 0 & \ddots & \ddots & 0 \\ 0 & 0 & 0 & \varepsilon_{n+1}^0 & \varepsilon_n^0 \\ 1 & 1 & \cdots & 1 & 1 \end{bmatrix} \cdot \begin{bmatrix} W_1 \\ W_2 \\ \vdots \\ \vdots \\ W_n \end{bmatrix} = \begin{bmatrix} \Delta P_2^0 - \Delta P_1^0 + \varepsilon_1^0 W_1^0 - \varepsilon_2^0 W_2^0 \\ \Delta P_3^0 - \Delta P_2^0 + \varepsilon_2^0 W_2^0 - \varepsilon_3^0 W_3^0 \\ \vdots \quad \vdots \quad \vdots \quad \vdots \\ \vdots \quad \vdots \quad \vdots \quad \vdots \\ \Delta P_n^0 - \Delta P_{n-1}^0 + \varepsilon_{n-1}^0 W_{n-1}^0 - \varepsilon_n^0 W_n^0 \end{bmatrix} \tag{3.22}$$

Sampaio (1985) applies the Cholesky method to the system 3.22 in order to calculate a new group of flow distribution values (W_1, W_2,...,W_n) starting from initial guess values (W_1^0, W_2^0,...,W_n^0). That iterative process is repeated until the following convergence criterion be met:

$$\sum_{i=1}^{n} \left| \frac{W_i^{(j)} - W_i^{(j-1)}}{W_i^{(j-1)}} \right| < \delta \tag{3.23}$$

where δ is the iterative process residual limit and j is the iteration counter.

Concerning the flow stability analysis, Sampaio (1985) correlates the pressure loss behavior in a reactor core (ΔP^*) with that one of each channel as follow:

$$\gamma = \frac{d\Delta P^*}{dW} = \left[\sum_{i=1}^{n} \frac{1}{(d\Delta P_i / dW_i)} \right]^{-1} \tag{3.24}$$

That correlation gives a way to evaluate flow stability where, for an initially downward flow undergoing a mass flow rate reduction process over time, while $\gamma > 0$, the flow is expected to remain stable with the same downward orientation in all the channels. However, when a $0 > \gamma > -\infty$ value is reached, it is possible the onset of instability and therefore a flow reversion in a hot channel. Accordingly, if that mass flow rate reduction process is continued and γ returns to a positive value ($\gamma > 0$) a flow reversion will necessarily happen.

3.2 CFX Three-Dimensional Modeling Formulation

In this section, the equation of mass, momentum and energy conservation solved by CFX are presented. Firstly, it is presented the instantaneous equation, applied when CFX is set to perform DNS (Direct Numerical Simulation). Furthermore, it is presented the $K-\omega$ and $K-\varepsilon$ formulations for turbulent flow scenarios, where those instantaneous equations are averaged leading to additional terms (ANSYS-INC, 2016a).

3.2.1 Governing Equations

3.2.1.1 Transport Equations

The instantaneous equation of mass, momentum, and energy conservation are defined as:

- The Continuity Equation

$$\frac{\partial \rho}{\partial t} + \nabla \cdot (\rho \mathbf{U}) = 0 \tag{3.25}$$

- The Momentum Equations

$$\frac{\partial (\rho \mathbf{U})}{\partial t} + \nabla \cdot (\rho \mathbf{U} \otimes \mathbf{U}) = -\nabla P + \nabla \cdot \boldsymbol{\tau} + \mathbf{S}_M \tag{3.26}$$

where $\boldsymbol{\tau}$ is the stress tensor for a newtonian fluid related to the strain rate by:

$$\boldsymbol{\tau} = \mu(\nabla \mathbf{U} + (\nabla \mathbf{U})^T - \frac{2}{3}\delta \nabla \cdot \mathbf{U}) \tag{3.27}$$

and δ is:

$$\delta = \begin{bmatrix} 1 & 0 & 0 \\ 0 & 1 & 0 \\ 0 & 0 & 1 \end{bmatrix}$$

- The Total Energy Equation

$$\frac{\partial \rho h}{\partial t} - \frac{\partial P}{\partial t} + \nabla \cdot (\lambda \nabla T) + \mathbf{U} \cdot \nabla P + \boldsymbol{\tau} : \nabla \mathbf{U} + \mathbf{S}_E \tag{3.28}$$

The term $\boldsymbol{\tau} : \nabla \mathbf{U}$, is always positive and is called the viscous dissipation.

For a compressible flow with low Mach number, the terms $\partial P/\partial t$ and $\mathbf{U} \cdot \nabla P$ can be neglected and the equation (3.28) becomes:

$$\frac{\partial \rho h}{\partial t} + \nabla \cdot (\rho \mathbf{U} h) = \nabla \cdot (\lambda \nabla T) + \boldsymbol{\tau} : \nabla \mathbf{U} + \mathbf{S}_E \tag{3.29}$$

3.2.1.2 Equations of State

The transport equations previously presented are complemented with constitutive equations of state for density and enthalpy in order to form a closed system. Those equations have the following form:

$$\rho = \rho(P,T) \tag{3.30}$$

$$dh = \left.\frac{\partial h}{\partial T}\right|_P \partial T + \left.\frac{\partial h}{\partial P}\right|_T \partial P = C_p \partial T + \left.\frac{\partial h}{\partial P}\right|_T \partial P \tag{3.31}$$

$$C_p = C_P(P,T) \tag{3.32}$$

3.2.1.3 Boussinesq Model

In CFX, for buoyant flows where the density variation is driven only by small temperature variations, the Boussinesq model is used. In this model, a constant reference density is used for all terms other than the buoyancy source term. The buoyancy source term is approximated as (ANSYS-INC, 2016b):

$$\rho - \rho_{ref} = -\rho_{ref}\ \beta(T - T_{ref}) \tag{3.33}$$

where β is the thermal expansivity:

$$\beta = -\frac{1}{\rho}\left.\frac{\partial \rho}{\partial T}\right|_P \tag{3.34}$$

and T_{ref} is the buoyancy reference temperature.

3.2.1.4 Transport Equations With the Boussinesq Model

The momentum equation (3.26) associated with the constitutive equation for newtonian fluids (3.27) gives the Navier-Stokes equation. Furthermore, for incompressible fluids, the equations (3.25), (3.26), and (3.27) can be written as follow:

$$\nabla \cdot \mathbf{U} = 0 \tag{3.35}$$

$$\rho \frac{\partial \mathbf{U}}{\partial t} + \rho \nabla \cdot (\mathbf{U} \otimes \mathbf{U}) = -\nabla P + \nabla \cdot \boldsymbol{\tau} + \mathbf{S}_M \tag{3.36}$$

$$\frac{\partial \rho h}{\partial t} + \rho \nabla \cdot (\mathbf{U} h) = \nabla \cdot (\lambda \nabla T) + \boldsymbol{\tau} : \nabla \mathbf{U} + \mathbf{S}_E \tag{3.37}$$

In such condition, due to the density be constant and C_p be only function of the temperature, the equations of state become:

$$\rho = \rho_{espec} \tag{3.38}$$

$$dh = C_p \partial T + \frac{\partial P}{\partial \rho} \tag{3.39}$$

$$C_p = C_P(T) \tag{3.40}$$

Thus, when the Boussinesq model is applied, the terms $\boldsymbol{\tau}$ and $\mathbf{S}_M$ of the transport

equations become:

$$\boldsymbol{\tau} = \mu(\nabla \mathbf{U} + (\nabla \mathbf{U})^T) \tag{3.41}$$

$$\mathbf{S}_{M,buoy} = \rho_{ref}\beta(T - T_{ref})\mathbf{g} \tag{3.42}$$

3.2.2 Turbulence Models

Turbulence are fluctuations in the flow field occurring in time and space. Its complexity is mainly due to its three-dimensional, unsteady and multi-scalar behavior. It occurs when the inertial forces in a flow become significant higher compared to the viscous forces, characterized by a high Reynolds number (ANSYS-INC, 2016c).

Navier-Stokes equations can describe both laminar and turbulent flows. However, typical turbulent flows oscillates on a large range of turbulent length and time scales that could be way smaller than the smallest finite volume mesh and in order to run a Direct Numerical Simulation (DNS) of these flows, it would require a very high computing power to the point that a simulation could not be viable anymore (ANSYS-INC, 2016c).

In that regard, turbulence models have been developed to deal statistically with effects of turbulence without the necessity of a substantial fine mesh and therefore high computational power (ANSYS-INC, 2016c).

3.2.2.1 Reynolds Averaged Navier-Stokes (RANS) Equations

Turbulence models try to solve a modified set of transport equations by using an averaged and a fluctuating component (ANSYS-INC, 2016d).

For instance, the velocity U_i can be decomposed into an average $\overline{U_i}$ and a time varying component u_i as follow:

$$U_i = \overline{U_i} + u_i \tag{3.43}$$

where:

$$\overline{U_i} = \frac{1}{\Delta t}\int_t^{t+\Delta t} U_i dt \tag{3.44}$$

The term Δt is a time scale large related to the turbulent fluctuations, but small related to the time scale that the equations are solved.

Substituting the averaged quantities into the transport equations previously presented, it results in the Reynolds averaged equations as follow:

$$\frac{\partial \rho}{\partial t} + \frac{\partial}{\partial x_j}(\rho U_j) = 0 \tag{3.45}$$

$$\frac{\partial \rho U_i}{\partial t} + \frac{\partial}{\partial x_j}(\rho U_i U_j) = -\frac{\partial P}{\partial x_i} + \frac{\partial}{\partial x_j}(\tau_{ij} - \rho\overline{u_i u_j}) + S_M \tag{3.46}$$

where τ is the molecular stress tensor that includes both the normal and the shear stress components.

The momentum and scalar transport equations contain now turbulent flux terms additional to the molecular diffusive fluxes and the Reynolds stresses term $\overline{u_i u_j}$, that arise from the nonlinear convective term in the un-averaged equations (ANSYS-INC, 2016d).

The Reynolds averaged energy equation is defined as:

$$\frac{\partial h_{tot}}{\partial t} - \frac{\partial P}{\partial t} + \frac{\partial}{\partial x_j}(\rho U_j h_{tot}) = \frac{\partial}{\partial x_j}(\lambda\frac{\partial T}{\partial x_i} - \rho\overline{u_j h}) + \frac{\partial}{\partial x_j}[U_i(\tau_{ij} - \rho\overline{u_i u_j})] + S_E \tag{3.47}$$

that differs to the instantaneous equation due to the term $\rho\overline{u_i u_j}$.

The mean total enthalpy is defined as:

$$h_{tot} = h + \frac{1}{2}U_i U_i + k \tag{3.48}$$

where k is the turbulent kinetic energy given by:

$$k = \frac{1}{2}\overline{u_i^2} \tag{3.49}$$

The additional variable may also be divided into an average component Φ and a time-varying component ϕ and becomes:

$$\frac{\partial \rho \Phi}{\partial t} + \frac{\partial}{\partial x_j}(\rho U_j \Phi) = \frac{\partial}{\partial x_j}(\Gamma \frac{\partial \Phi}{\partial x_j} - \rho \overline{u_i \phi}) + S_M \tag{3.50}$$

3.2.2.2 Two Equation Turbulence Models

Two-equation turbulence models are very widely used, once they provide a good balance between accuracy and computational power demanded. In those models, both the velocity and length scale are solved using separate transport equations.

According to the CFX-Solver Theory Guide, in two-equation models, the turbulence velocity scale is computed from the turbulent kinetic energy, which is provided from the solution of its transport equation (ANSYS-INC, 2016e). The turbulent length scale is estimated from two properties of the turbulence field, usually the turbulent kinetic energy and its dissipation rate. The dissipation rate of the turbulent kinetic energy is provided from the solution of its transport equation.

3.2.2.3 The k-epsilon Model in ANSYS CFX

The turbulence kinetic energy k is defined as the variance of the fluctuations in velocity has dimensions of (L^2T^{-2}). The turbulence eddy dissipation ε and is defined as the rate at which the velocity fluctuations dissipate with dimensions of k per unit time, L^2T^{-3} (ANSYS-INC, 2016e).

The continuity and momentum equation are defined in the $k-\varepsilon$ model as:

$$\frac{\partial \rho}{\partial t} + \frac{\partial}{\partial x_j}(\rho U_j) = 0 \tag{3.51}$$

$$\frac{\partial \rho U_i}{\partial t} + \frac{\partial}{\partial x_j}(\rho U_i U_j) = -\frac{\partial P'}{\partial x_i} + \frac{\partial}{\partial x_j}(\mu_{eff}(\frac{\partial U_i}{\partial x_j} + \frac{\partial U_j}{\partial x_i}) + S_M \tag{3.52}$$

where μ_{eff} is the defined by:

$$\mu_{eff} = \mu + C_\mu \rho \frac{k^2}{\varepsilon} \tag{3.53}$$

and C_μ is a constant.

Values for k and ε come directly from the differential transport equations for the turbulence kinetic energy and turbulence dissipation rate:

$$\frac{\partial(\rho k)}{\partial t} + \frac{\partial}{\partial x_j}(\rho U_j k) = \frac{\partial}{\partial x_j}\left[\left(\mu + \frac{\mu_t}{\sigma_k}\right)\frac{\partial k}{\partial x_j}\right] + P_k - \rho\varepsilon + P_{kb} \tag{3.54}$$

and

$$\frac{\partial(\rho\varepsilon)}{\partial t} + \frac{\partial}{\partial x_j}(\rho U_j \varepsilon) = \frac{\partial}{\partial x_j}\left[\left(\mu + \frac{\mu_t}{\sigma_\varepsilon}\right)\frac{\partial \varepsilon}{\partial x_j}\right] + \frac{\varepsilon}{k}(C_{\varepsilon 1}P_k - C_{\varepsilon 2}\ \rho\varepsilon + C_{\varepsilon 1}P_{\varepsilon b}) \tag{3.55}$$

where $C_{\varepsilon 1}$, $C_{\varepsilon 2}$, σ_k and σ_ε are constants and P_k, P_{kb}, $P_{\varepsilon b}$ represent the influence of the buoyancy forces (ANSYS-INC, 2016e).

3.2.2.4 The k-omega Model in ANSYS CFX

According to the Ansys theory guide, one of the advantages of the $k-\omega$ formulation is the near-wall treatment for low-Reynolds number computations. The model does not involve the complex nonlinear damping functions required for the $k-\varepsilon$ model and is, therefore, more accurate and more robust. A low-Reynolds $k-\varepsilon$ model would typically require a near-wall resolution of $y^+ < 0.2$, while a low-Reynolds number $k-\omega$ model would require at least $y^+ < 2$. The $k-\omega$ model assumes that the turbulence viscosity is linked to the turbulence kinetic energy and turbulent frequency via the relation (ANSYS-INC, 2016e):

$$\mu_t = \rho\frac{k}{\omega} \tag{3.56}$$

The $k-\omega$ model solves two transport equations. One related to the turbulence kinetic energy "k":

$$\frac{\partial(\rho k)}{\partial t} + \frac{\partial}{\partial x_j}(\rho U_j k) = \frac{\partial}{\partial x_j}\left[\left(\mu + \frac{\mu_t}{\sigma_k}\right)\frac{\partial k}{\partial x_j}\right] + P_k - \beta'\rho k\omega + P_{kb} \tag{3.57}$$

and another related to the turbulent frequency "ω":

$$\frac{\partial(\rho\omega)}{\partial t} + \frac{\partial}{\partial x_j}(\rho U_j k) = \frac{\partial}{\partial x_j}\left[\left(\mu + \frac{\mu_t}{\sigma_\omega}\right)\frac{\partial \omega}{\partial x_j}\right] + \alpha\frac{\omega}{k}P_k - \beta\rho\omega^2 + P_{\omega b} \tag{3.58}$$

The density and velocity vector, ρ and $\mathbf{U}$ respectively, are treated as known quantities from the Navier-Stokes method. The model constants are defined as:

$$\beta' = 0.09$$
$$\alpha = 5/9$$
$$\beta = 0.075$$
$$\sigma_k = 2$$
$$\sigma_\omega = 2$$

The unknown Reynolds stress tensor term, $\rho\overline{u_i u_j}$, is given by:

$$\rho\overline{u_i u_j} = \mu_t\left(\frac{\partial U_i}{\partial x_j} + \frac{\partial U_j}{\partial x_i}\right) - \frac{2}{3}\delta_{ij}\left(\rho k + \mu_t\frac{\partial U_k}{\partial x_k}\right) \tag{3.59}$$

4 Flow Simulations

In this chapter, it is presented the steps of the three-dimensional CFX simulations performed, which the results are afterward compared against those ones obtained from Sampaio's FORTRAN program (based in his unidimensional model). A full set of qualification steps performed in order to ensure adequate choices of meshes and turbulence closure models are presented. An experiment in a test section with two parallel channels performed by Sampaio in a previous study is replicated. Furthermore, it is presented a 3D four channels downward flow simulation performed in CFX in order to evaluate the accuracy of the 1D flow model predictions in that configuration.

4.1 CFX Model Qualification

The qualification procedures for mesh and turbulence models consisted basically in comparing friction factor and entrance length obtained from simulations of an internal viscous flow through a pipe in CFX against appropriated correlations. Furthermore, it is presented a mesh convergence analysis performed as a final verification prior to the flow simulations themselves, addressed in the next section.

4.1.1 Channel Geometry Modeling and Flow Parameter Setting

It was used a dimensionless approach when defining fluid properties and flow geometry to be simulated. That expressively simplifies the simulation process once all parameters are set to be one unit, but the viscosity, set to be the inverse value of Reynolds number intended to be simulated. The pipe length was defined as 200. In summary:

$$\upsilon = 1$$

$$\rho = 1$$

$$\mu = 1/Re$$

$$D = 1$$

$$L = 200$$

4.1.2 Channel Mesh Modeling

Hexahedral elements were chosen to compose the mesh due to its better accuracy and geometric compatibility with a cylindrical channel form. The Reynolds number was estimated not being greater than 15×10^3 at any time during the CFX simulations performed in this study. Therefore, that value was considered to determine the thickness of the first layer of the mesh in the near-wall domain. That was calculated using $U = 1$; $\rho = 1$; $\mu = (15 \times 10^3)^{-1}$; $L = 1$; $y^+ = 1$, desired value for near-wall modeling according to Salim and Cheah (2009), by following the steps of equations below:

$$Re_x = \frac{\rho U_\infty L}{\mu} \tag{4.1}$$

$$C_f = \frac{0.026}{Re_x^{1/7}} \tag{4.2}$$

$$\tau_{wall} = \frac{C_f \rho U_\infty^2}{2} \tag{4.3}$$

$$U_{fric} = \sqrt{\frac{\tau_{wall}}{\rho}} \tag{4.4}$$

$$\Delta s = \frac{y^+ \mu}{U_{fric} \rho} \tag{4.5}$$

It resulted in $\Delta s = 0.00116206$, that was truncated to 0.001 afterward.

4.1.3 Laminar Flow Regime Analysis

This section covers a preliminary study made with a simplified mesh designed for the laminar flow range domain in order to test the general parameter setting of the modeling process in CFX software. However, it's worth mentioning that the full meshing process performed for the main simulations study is covered later on in this work (subsection 4.1.5).

The first procedure consisted in comparing the entrance length of the laminar flow

simulated in CFX against the Durst et al. (2005) correlation, shown below:

$$X_D/D = [(0.619)^{1.6} + 0.0567Re^{1.6})]^{1/1.6} \tag{4.6}$$

CFX was set to perform a DNS (Direct Numerical Simulation), in which Navier-Stokes equations are solved without any turbulence model assistance.

4.1.3.1 Laminar Flow Entrance Length Measuring

Another verification procedure concerning the 3D CFX modeling consisted of comparing if the entrance length of the simulated flow agrees with the reference correlation for a group of Reynold number. In order to do that it was necessary to define a measurement criterion: the length, starting on the inlet surface, for which the velocity over the center line of the flow is equal to 0.99 of the velocity on the outlet surface.

The pipe length was defined as 200. That value was necessary because it was noted that small variations in the length of the fully developed referential-velocity point could lead to a significant deviation of the real entrance length. Thus, a point far enough from the fluid inlet was selected to assure the velocity there was significantly developed.

It was performed simulations for Reynolds number of 100, 200, 500 e 1000. As shown in Fig. 7, it can be seen a strong agreement between CFX simulations and the reference correlation for entrance length values.

Figure 7 – Entrance Length vs Reynolds Number

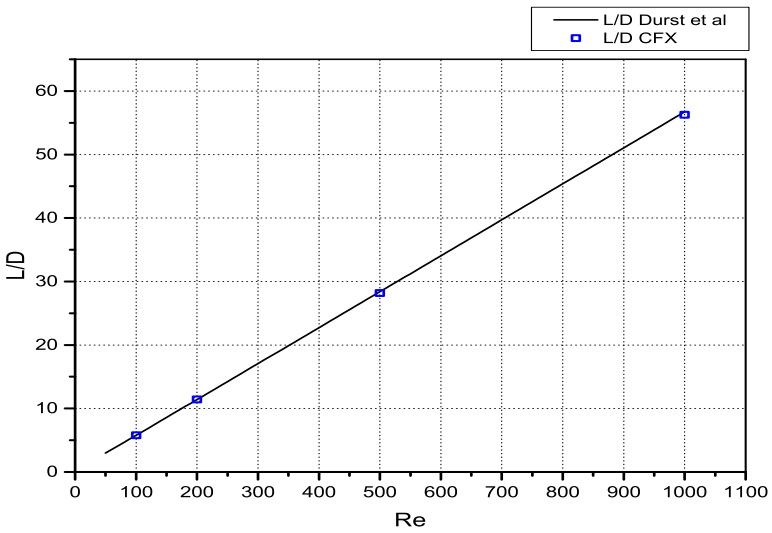

Source: Author.

4.1.3.2 Laminar Flow Friction Factor Measuring

This part of the qualification procedure consisted in comparing the friction factor of laminar flows simulated in CFX against the $64/Re$ correlation. The friction factor was calculated with the following equation:

$$f = \frac{-(dp/dx)D}{1/2\rho\mu_m^2} \tag{4.7}$$

It was performed simulations for Reynolds number of 100, 200, 500 e 1000. As shown in Fig. 8, it can be seen a strong agreement between friction factor values of CFX simulations and 64/Re correlation.

It was also observed that at the fully developed velocity profile, the max velocity was 2.0006, roughly 0.03% of deviation from the expected value for a laminar flow of two times the initial velocity (FOX et al., 2006).

Figure 8 – Friction Factor vs Reynolds Number

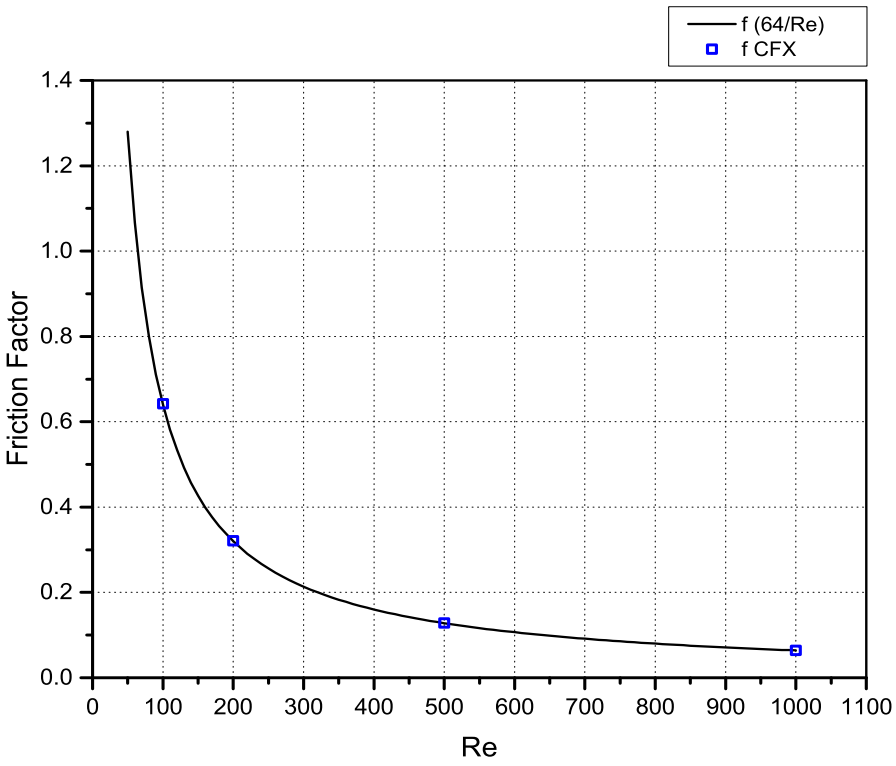

Source: Author.

4.1.4 Turbulent Flow Regime Analysis

This part of the qualification procedure consisted in comparing the friction factor of the turbulent flows simulated in CFX against the Blasius correlation for smooth wall pipes, shown below:

$$f = 0.316 Re^{-\frac{1}{4}} \tag{4.8}$$

Once again, it was used the equation (4.7) to calculate the friction factor of the CFX simulations. It was performed turbulent flow simulations for Reynolds number of 5000, 7500, 10000, 12500 and 15000 using both $k-\omega$ and $k-\epsilon$ turbulence models. The mesh settings used here correspond to the mesh number 5, presented in the next section. The results are shown in the following chart:

Figure 9 – Friction Factor vs Reynolds Number

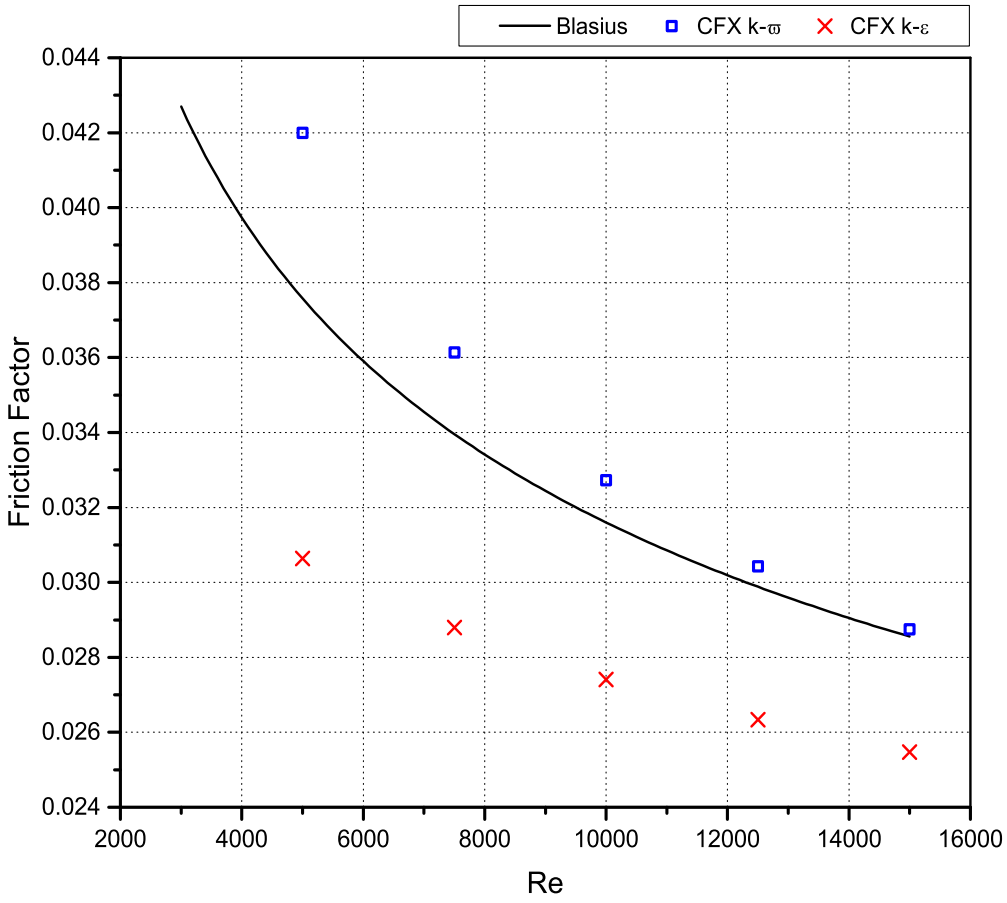

Source: Author.

As shown in the above chart, it can be seen that $k-\omega$ turbulence model had a better agreement with Blasius correlation than $k-\varepsilon$ one. It had a deviation of roughly 10% at $Re = 5000$ that gradually decreases to roughly zero, as the Reynolds number rises.

4.1.5 Mesh Optimization

The mesh quality used in a simulation is directly related to the final solution accuracy. However, the use of refinement above that necessary for a given flow simulation can result in a significant increase of computational power demanded to reach a solution within a reasonable time. Thus, to prevent the use of an overrefined mesh, it was performed a study consisting of comparing the friction factor of 5 mesh refinement levels against the reference value given by Blasius correlation. Fig. 10 shows those refinement levels.

Besides the low refinement used in some cases, all the tested meshes respected the thickness value of the first layer $\Delta s = 0.001$. Table 1 shows the tested meshes data and the deviation result from the Blasius correlation for a flow simulation with Reynolds number equal to 15000.

Table 1 – Meshes Data

Mesh	Nodes	Elements	Min. Orthogonal Quality	Max. Skewness	Fric. Factor	Deviation
1	29161	26880	0.1276	0.40117	0.03188	11.6%
2	58996	55500	0.14658	0.41028	0.03011	5.4%
3	186465	179200	0.29189	0.43354	0.02898	1.5%
4	509648	495000	0.68212	0.44821	0.02864	0.3%
5	1615345	1579200	0.74449	0.45777	0.02875	0.7%

Source: Author.

According to the above table, it can be noted that mashes 1 and 2 had a remarkable deviation from the reference value. Furthermore, the chosen mesh to be used from now on in this work (nº 4) had a good agreement but with roughly 3 times fewer elements than the fifth one. Thus, the mesh to be used in the simulations was set to have $0.2D$ length elements along its axial direction and 44 angular divisions in its cross-section.

Figure 10 – Channel Modeled Mashes

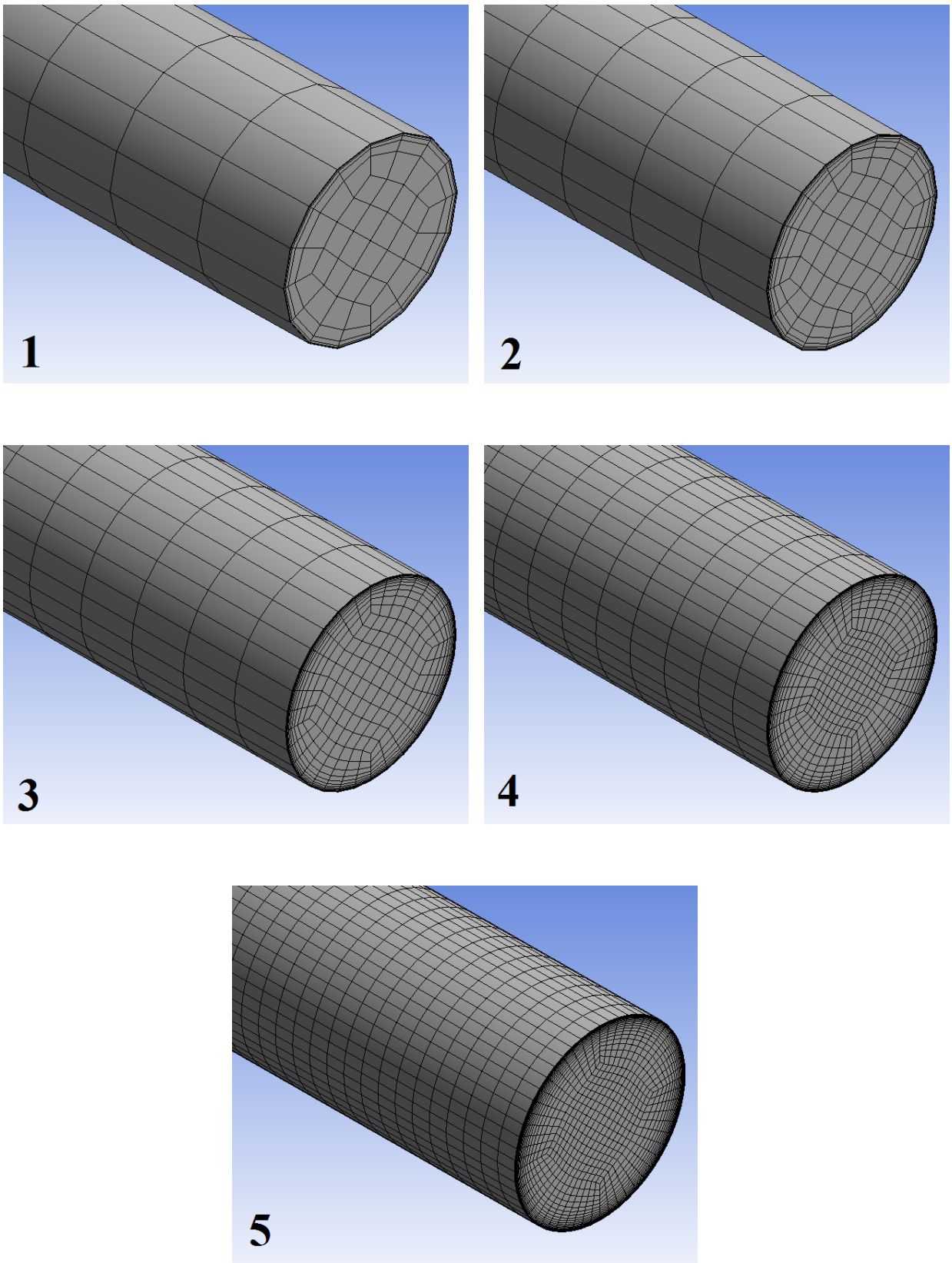

Source: Author.

4.2 Downward Flow Through Two Channels Simulation

In his work, Sampaio performed a downward flow through two channels experiment in order to analyze the agreement between its results and that one predicted by his simplified model regarding flow stability. In this section, it is presented a similar study concerning of performing a 3D CFX simulated version of that experiment.

4.2.1 Sampaio's Experiment Description

The experimental framework comprised two metallic pipes with the same diameter connected to an upper and a lower parallelepipedal plenums. The upper plenum had two lateral inlets and the lower plenum had one inferior outlet. That assembly was attached to a water circuit with an adjustable pump and a flow rate meter. Both pipes could be heated by independent electrical resistances attached to the external surface of them. On the ends of each pipe, there were thermocouples installed to measure the temperature difference between the start and the end point of each pipe. That temperature difference measure was the way Sampaio used to know the flow orientation inside the pipe. Once the fluid got hotter as it passed through the heated pipe, it was expected to exit the channel with a higher temperature than that one it had when it got in, and a positive difference temperature signal was expected to be indicated. Equivalently, once a reversion flow was established, a negative difference temperature signal was expected to be indicated.

The experiment to be replicated in CFX consisted in setting a given heating power to the hot channel, no heating power to the cold one and a given initial flow rate in the circuit so that it is observed a downward flow condition indication inside the hot channel. After that, the initial flow rate was gradually reduced until it was indicated a negative signal of temperature difference in the hot channel, meaning the onset of a flow reversion in the hot pipe. Fig. 11(a) shows the described experimental assembly. The two possible flow configuration for that experiment are schematically described in the Fig. 11(b), downward flow in both pipes with a reduced flow rate in the hot one, and Fig. 11(c), upward flow in the hot pipe.

Figure 11 – (a)Assembly (b)Downward flow scheme (c)Upwardflow scheme

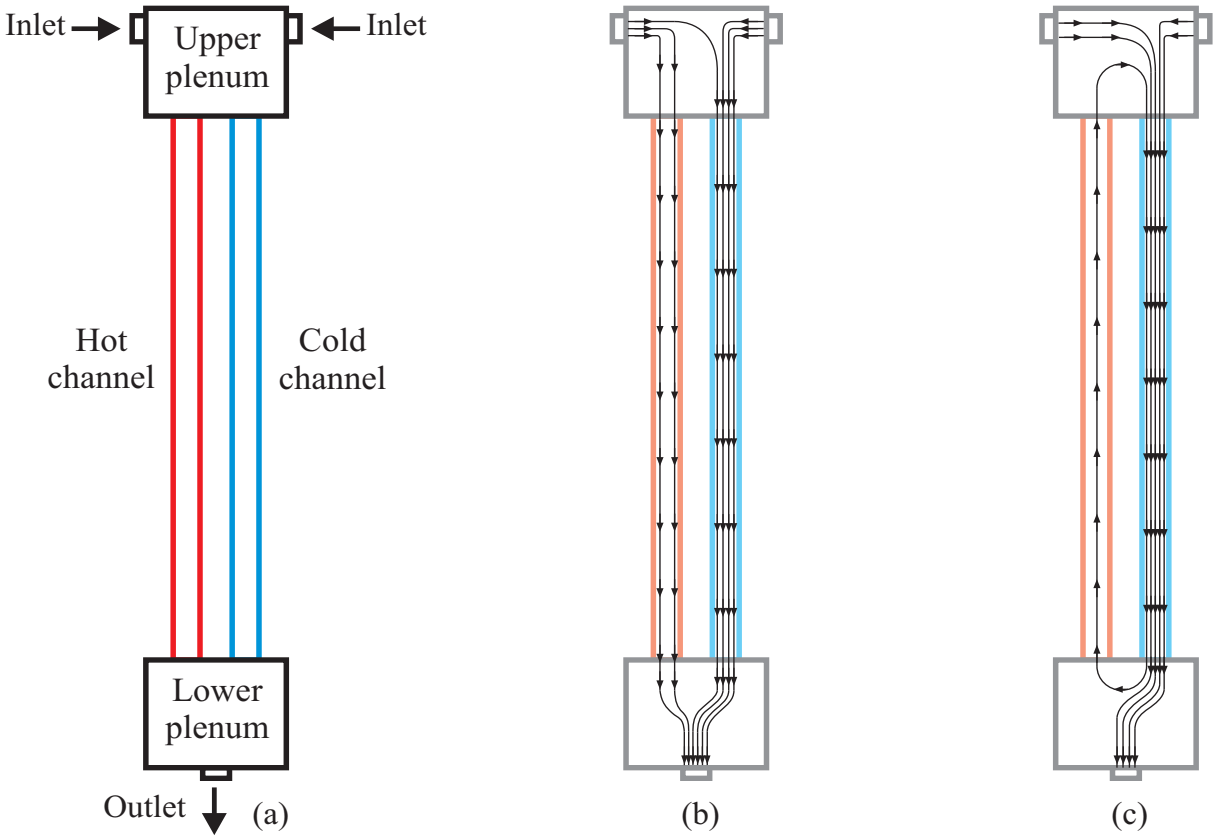

Source: Author.

4.2.2 CFX Modeling

Differently from the dimensionless approach used at the qualification phase, now all the original dimensions of Sampaio's experiment were totally applied in the flow geometries modeling, as well as the fluid proprieties (water). The channels were $0.05m$ in diameter and $1m$ length. Two extensions of the fluid inlets were placed in order to develop the flow prior to it gets into the upper plenum. A secondary geometry was made aiming to perform the analysis of the potential influence of the plenum format and size on the stability results. Fig. 12 shows the final geometries. Regarding the channels mesh, all the qualified elements dimensions and settings were due converted and applied at this phase.

The $k-\omega$ turbulence model was chosen due to its better performance over $k-\varepsilon$ for friction factor in the Reynolds range previously tested. Moreover, it is in accordance with the Ansys Theory Guide recommendation concerning the experiment flow conditions, where it states that one of the advantages of the $k-\omega$ formulation is the near-wall treatment for low-Reynolds number computations (ANSYS-INC, 2016e).

Figure 12 – CFX Model Geometries

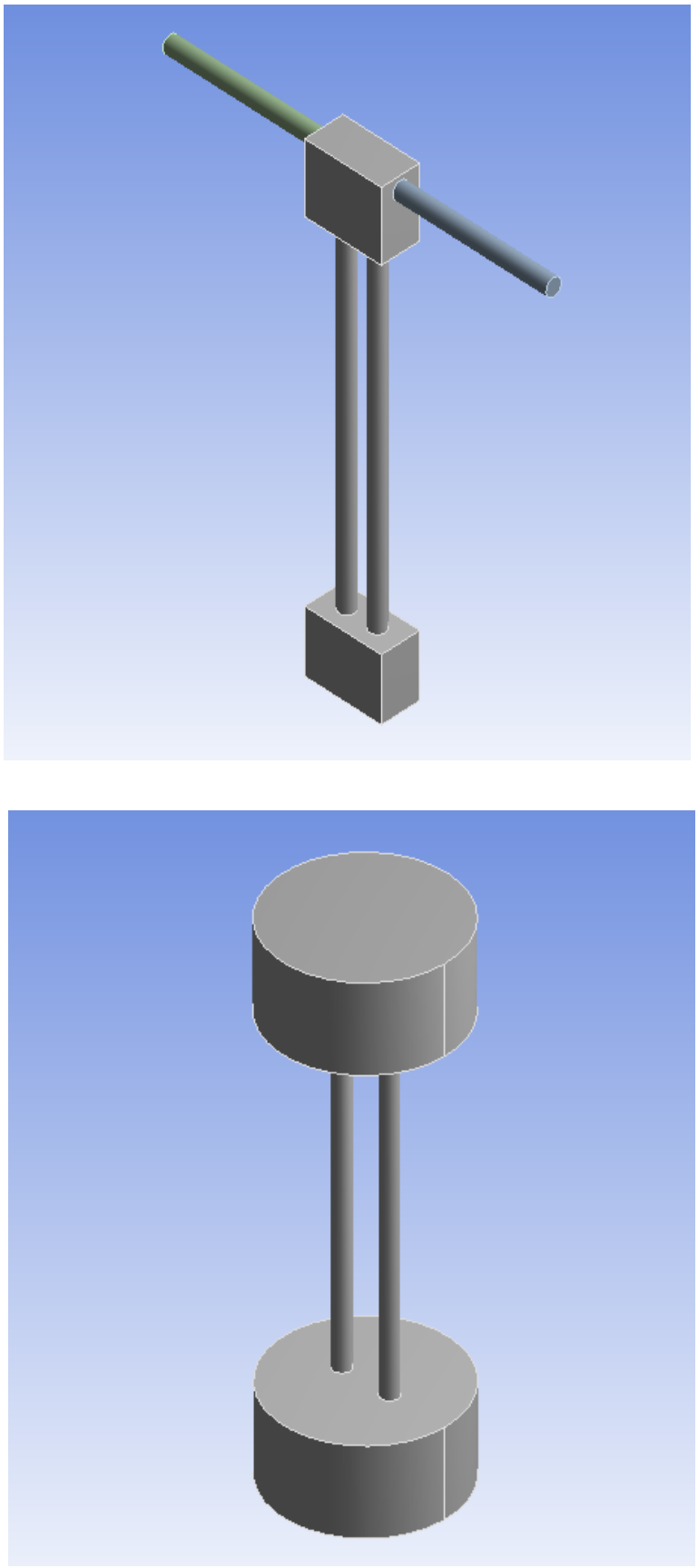

Source: Author.

4.2.3 CFX Simulations

The simulations were carried out within three rounds where the hot channel external surface was set to receive 1700, 1088 and 425W for each round respectively. No heating power was set to the cold channel. Those heating powers were uniformly distributed over the external flow surface, i.e., uniform heat flux ($q''(z) \approx< q''(z) >$). For each round, the simulations started with a total mass flow rate great enough to a downward flow in the hot channel to be established. Then, successive simulations with decreasing steps of 0.0025Kg/s were carried out until a flow reversion in the hot channel be observed.

4.2.3.1 Plenum Geometry and Heat Flux Profile Influence Analysis

In addition to the regular simulations, it was carried out a study to determine if the size or shape of the plenum or the heat flux profile along the Z axis of the hot channel would influence the final instabilities results. Those studies were carried out with 1088W heating power being applied.

In order to analyze a possible plenum influence in the simulations, it was created a plenum geometry that could provide a large flow volume and thereby minimize any eventual influence a small plenum could have on the simulations results. It is worth mentioning that is a more similar condition to that occurring in a real pool-type reactor core. Hence, it was created a plenum with 10D in diameter (0.5m) and 5D height (0.25m). The Fig. 12 shows the final geometry.

Moreover, another set of simulations aiming to analyze a possible heat flux profile influence on instability results was carried out. Therefore, it was set a cosinusoidal heat flux profile along de Z axis, on the channel surface. The heat flux profile was defined by the following equation:

$$q''(z) = q''_{max} cos\left[\frac{\pi z}{L_e} - \pi\left(\frac{L_e + 2h_p}{2L_e}\right)\right] \tag{4.9}$$

where:

q''_{max} is the peak heat flux (approximately $10885 W/m^2$)

L_e is the channel length ($L = 1m$)

h_p is the plenum height ($h_p = 0.18m$)

$\pi\left(\frac{L_e + 2h_p}{2L_e}\right)$ is a coordinate adjust term

4.3 Downward Flow Through Four Channels Simulation

This section aims to step up the analysis toward a more similar condition to that one possible to occur in a real reactor core. Therefore, now it is presented a round of four-channels downward flow CFX simulations that were performed to evaluate the agreement of results obtained with CFX 3D model and those ones predicted by Sampaio's 1D model. Besides of instabilities mass flow rate points, now it is also analyzed the flow distribution results.

4.3.1 CFX Modeling

In the modeling phase it was applied the same approach used in the previous two-channels simulations. The channels were geometrical identically to that one used in the previous simulations, i.e., $0.05m$ in diameter and $1m$ length, as well as were the mesh and the turbulence model ($k-\omega$) and fluid properties (water).

The channels were placed in a rectangular array on the plenums. Regarding the size and geometry of the plenums, in order to reduce the computational power demanded to solve these larger simulations, it was designed two small cylindrical plenums. It is worth mentioning this strategy was applied after the previous simulations have indicated the plenum geometries having no significant influence on the flow instabilities results. Fig. 13 shows the lower plenum final geometry.

Figure 13 – CFX Four-Channels Lower Plenum

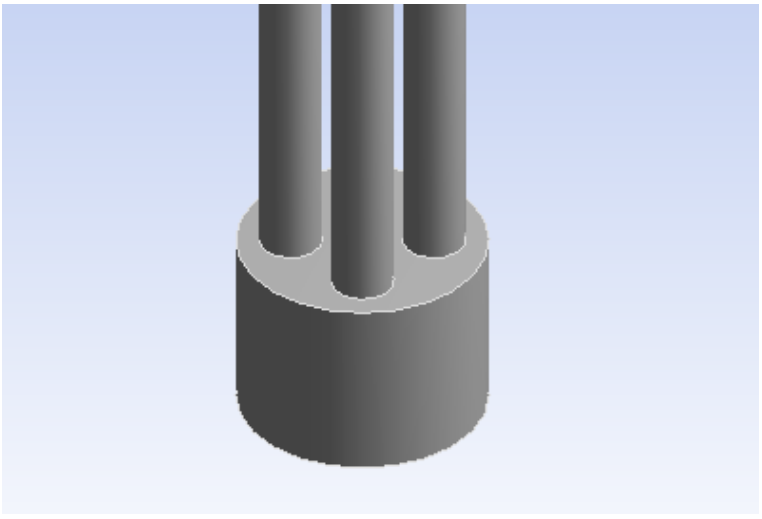

Source: Author.

4.3.2 Simulation Description

The simulations consisted of setting a given heating power to each channel and a given initial total mass flow rate in the circuit so that it was observed a downward flow condition inside all the channels. After that, successive simulations with decreasing steps of 0.5Kg/s were carried out until a flow reversion in the hot channel occur.

The entrance temperature was set to 50°C. The heating power was uniformly distributed over the external flow surface, i.e., uniform heat flux ($q''(z) \approx < q''(z) >$) according to the Tab. 2. Fig. 14 shows the schematic arrange of the flow cross-section for the first round of simulations.

Table 2 – Heating Power by Channel

Round	CH1	CH2	CH3	CH4
1	3000W	1500W	200W	1000W
2	1500W	750W	100W	500W
3	300W	150W	20W	100W

Source: Author.

Figure 14 – Schematic Arrange of the Flow Cross-Section (Round 1)

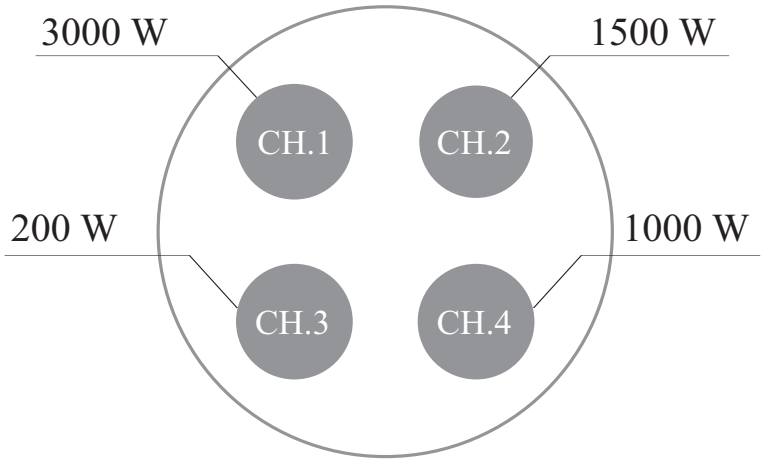

Source: Author.

5 Results and Discussion

5.1 Downward Flow Through Two Channels

Concerning the standard-replication of Sampaio's experiment, for both flow conditions, i.e., downward flow in the hot (left) channel and reverse downward flow in the hot (left) channel, the Fig. 15 shows a 3D velocity rendering of the flow after the reversion onset. Fig. 16 shows the upper plenum middle cross-section velocity chart and Fig. 17 shows the temperature distribution chart. The chart (downward flow in the hot channel) underwent to a 0.2500 Kg/s and bottom chart (reverse upward flow in the hot channel) was underwent to 0.2550 Kg/s of the total mass flow rate. For both simulations, the hot channel received 1088W of heating power.

As can be seen, the simulation resulted in flows patterns very similar to that theoretically expected, i.e., a high-velocity profile in the cold channel after a reverse flow be established in the hot channel.

Table 3 shows the total mass flow rate reversion point results of Sampaio's 1D model, Sampaio's experiment and CFX 3D model.

Table 3 – Mass Flow Rate of the Last Downward Flow Stable Event

Source	425W	1088W	1700W
Sampaio's Experiment	0.1510 Kg/s	0.2030 Kg/s	0.2270 Kg/s
Sampaio's 1D Model	0.1803 Kg/s	0.2480 Kg/s	0.2895 Kg/s
CFX 3D Model	0.1825 Kg/s	0.2525 Kg/s	0.2925 Kg/s

Source: Author.

Fig. 18 shows the instabilities results. In the X-axis is the hot channel heating power, and in the Y-axis is the total mass flow rate.

Concerning the influence of heat flux and plenum shape/size, the table 4 shows the resulted mass flow rate point of stable downward flow obtained for each situation. Furthermore, Fig. 18 shows that instabilities results in a chart. In the X-axis is the hot channel heating power, and in the Y-axis is the total mass flow rate.

Table 4 – Plenum Geometry and Heat Flux Profile Influence

Source	Mass Flow Rate
Sampaio's 1D Model	0.2480 Kg/s
CFX 3D (Par. Plenum)	0.2525 Kg/s
CFX 3D (Cyl. plenum)	0.2550 Kg/s
CFX 3D (Cyl. Plenum + Coss. H.F.)	0.2500 Kg/s

Source: Author.

Figure 15 – Upper Plenum After-Reversion Velocity Volume Rendering - 1088 W

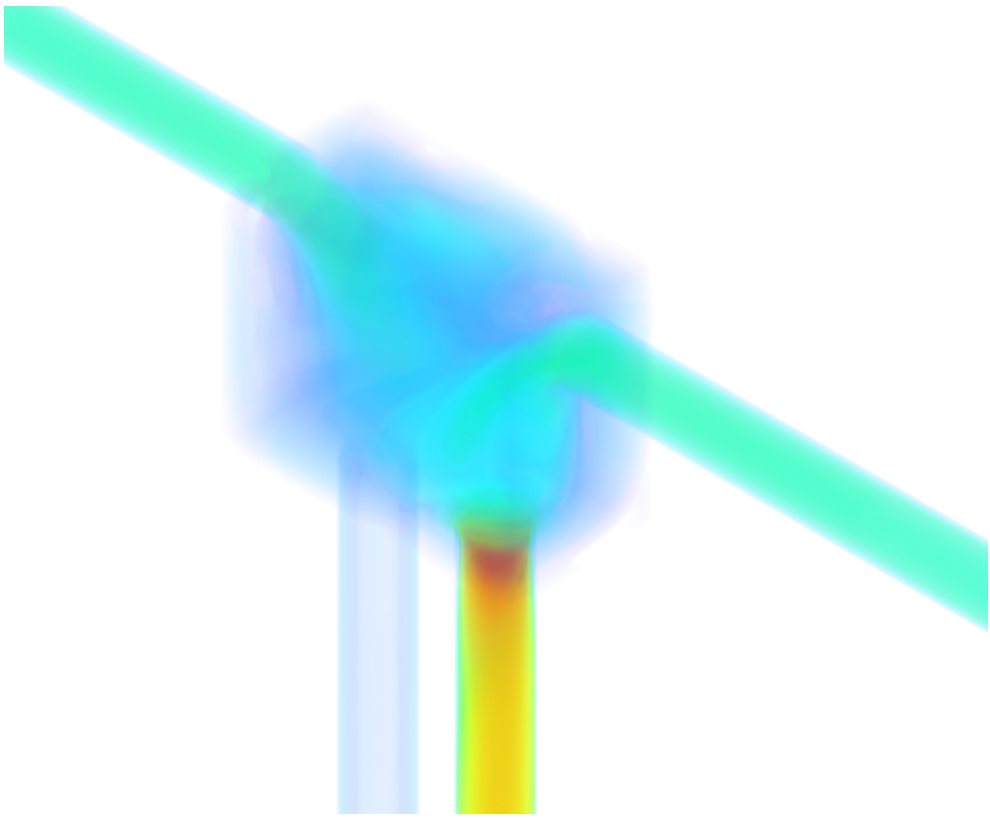

Source: Author.

Figure 16 – Upper Plenum Middle Cross-Section Velocity Chart - 1088W. Top: Downward Flow in the Hot Channel. Bottom: Reverse Flow in the Hot Channel.

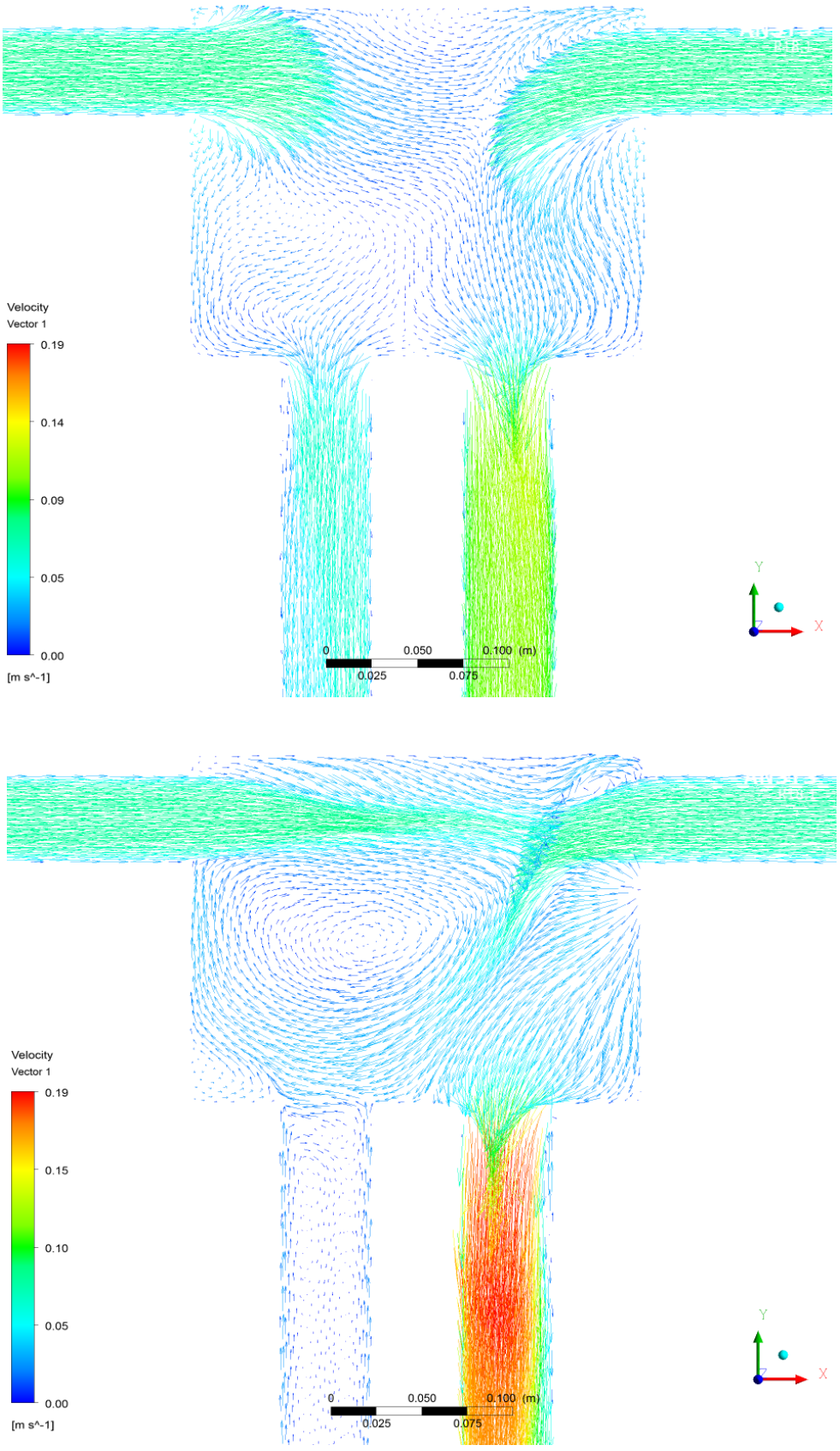

Source: Author.

Figure 17 – Flow Middle Cross-Section Temperature Chart - 1088W. Top: Downward Flow in the Hot Channel. Bottom: Reverse Flow in the Hot Channel.

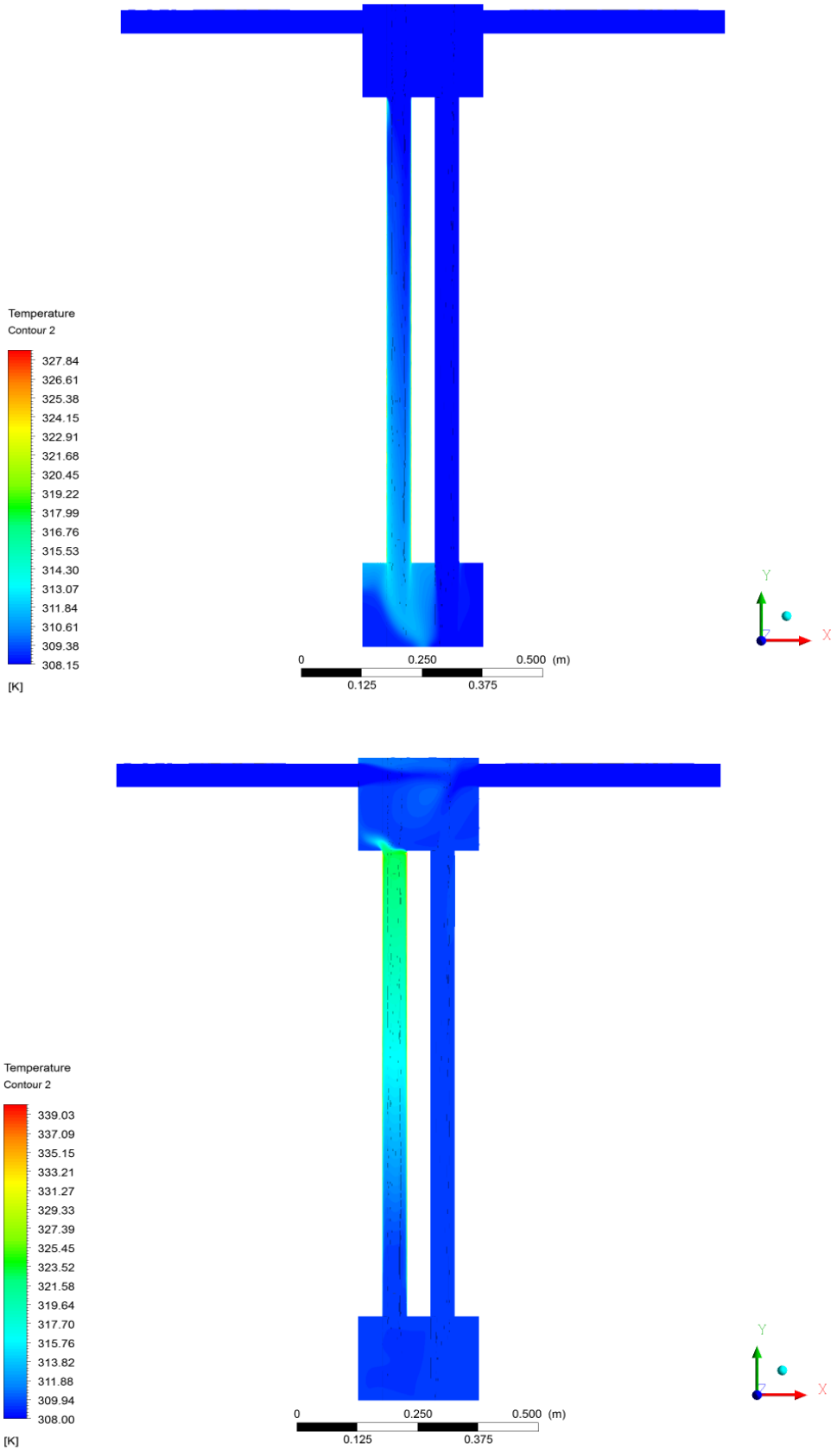

Source: Author.

Figure 18 – Top: Instability Chart. Botton: Plenum Geometry and Heat Flux Analysis

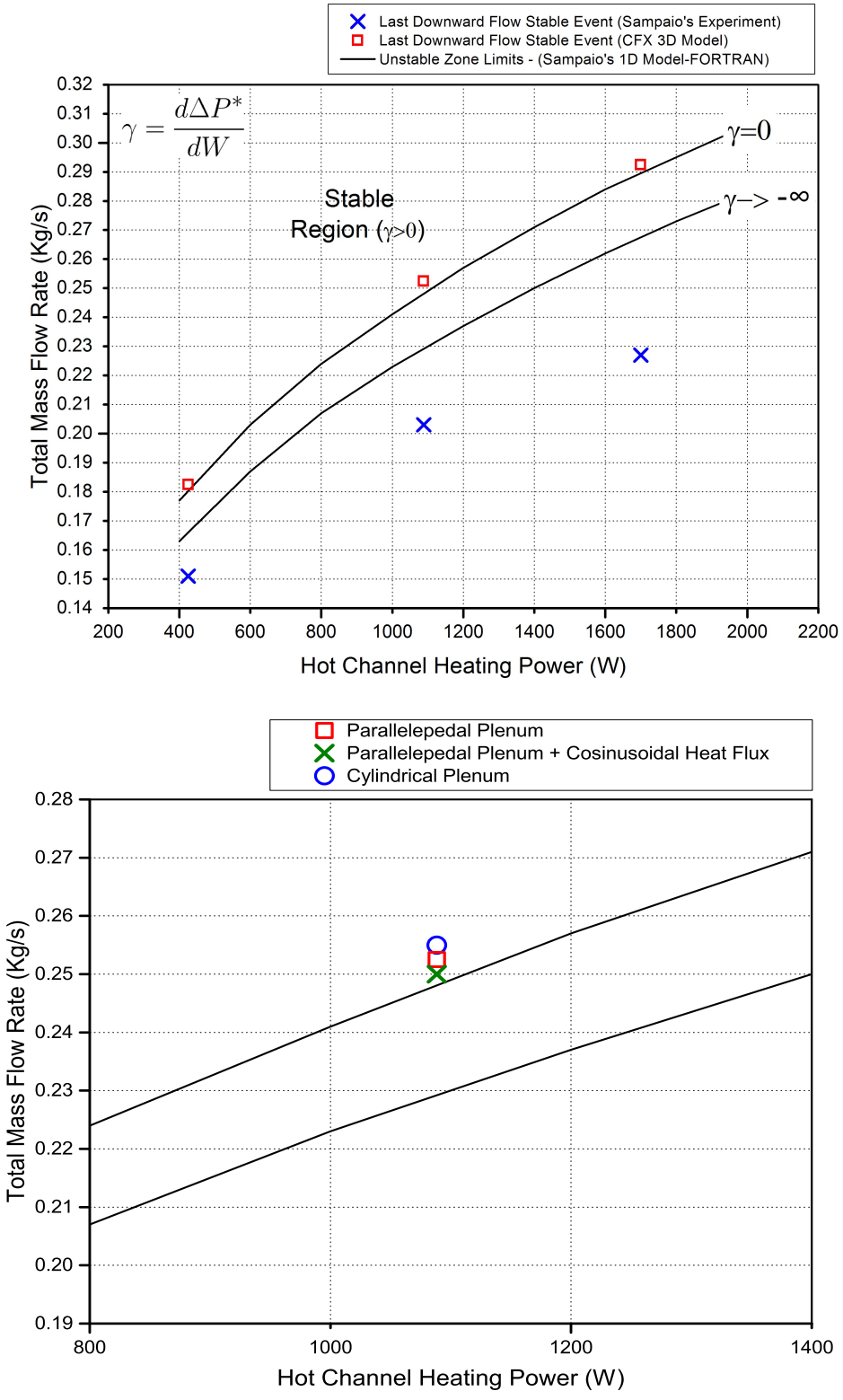

Source: Author.

In the above results, it can be observed a strong agreement between 3D CFX Simulations and 1D Sampaio's model prediction, as shown in Fig. 18. Nevertheless, it can be noted a significant discrepancy from those results to that one Sampaio obtained with his experiment. A possible reason for that is a deviation in the water physical properties values used in the CFX simulations from that one of the Sampaio used in this experiment. A second hypothesis concerns measurement deviations of Sampaio's experiment due to the difficulty in detecting a flow reversion based in a temperature difference signal, likely to create some delayed response.

5.1.1 Plenum Geometry and Heat Flux Profile Influence Analysisn

In the results of the of the Plenum Geometry and Heat Flux Profile influence study, the reversion points are fairly grouped with less than 1% deviation from average for each case. Hence, that indicates there is no relevant influence of those parameters in the final results.

5.2 Downward Flow Through Four Channels

It was analyzed the flow distribution of each channel with charts correlating the total (circuit) mass flow rate and the channel mass flow rate as can be seen in the figures 19, 20 and 21. The blue lines represent Sampaio's 1D model and red ones the 3D CFX results.

Figure 19 – Flow Distribution Charts - Round 1

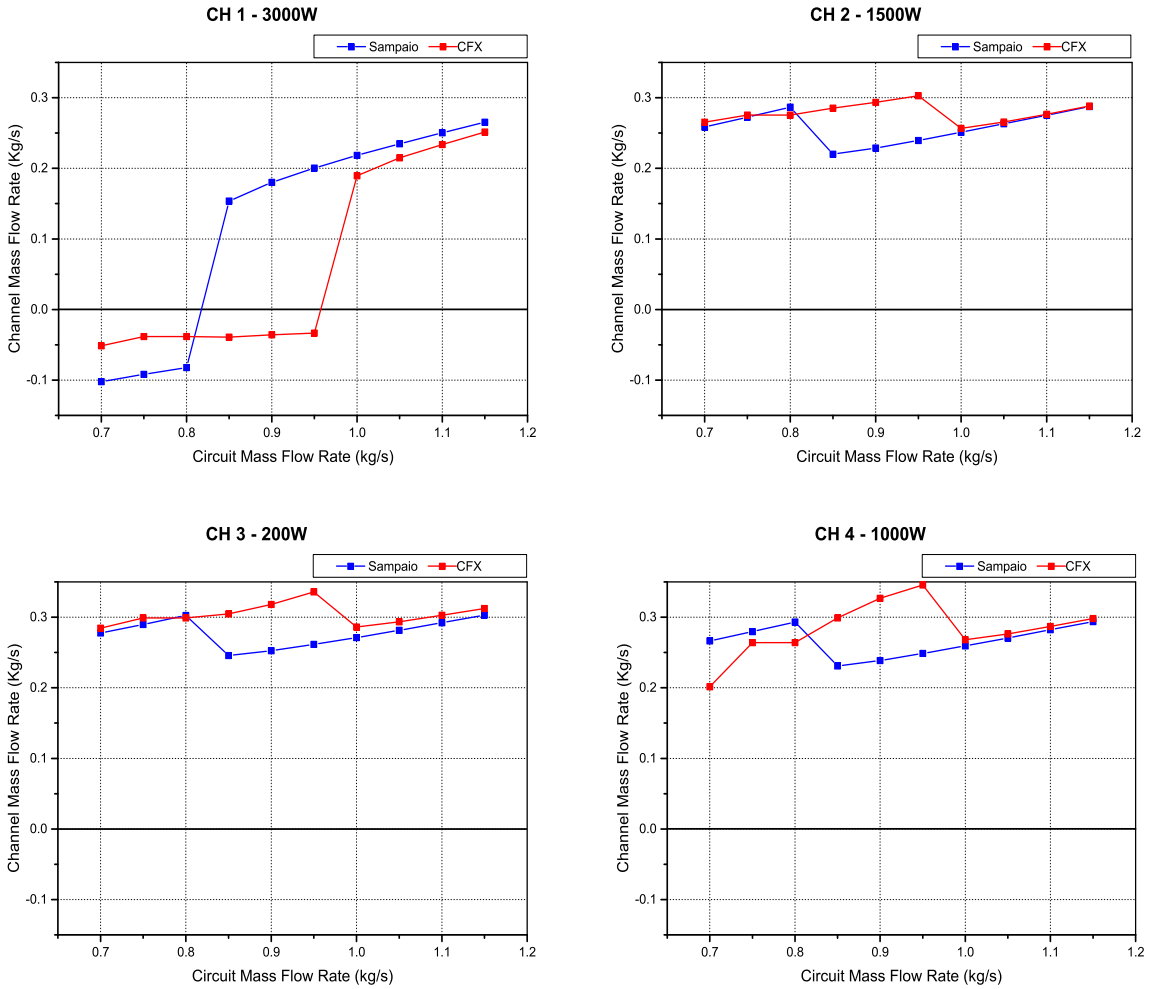

Source: Author.

Table 5 – 1D vs CFX 3D - Mass Flow Rate (Kg/s) results by Channel - Round 1

W_T	W_1		W_2		W_3		W_4	
	Sampaio	CFX	Sampaio	CFX	Sampaio	CFX	Sampaio	CFX
0.70	-0.1023	-0.0515	0.2585	0.2654	0.2775	0.2845	0.2663	0.2014
0.75	-0.0917	-0.0382	0.2725	0.2755	0.2897	0.2988	0.2795	0.2639
0.80	-0.0823	-0.0382	0.2868	0.2755	0.3025	0.2988	0.2931	0.2639
0.85	0.1536	-0.0392	0.2199	0.2854	0.2456	0.3048	0.2309	0.2989
0.90	0.1802	-0.0358	0.2286	0.2936	0.2525	0.3181	0.2387	0.3267
0.95	0.2004	-0.03338	0.2395	0.3027	0.2614	0.3357	0.2487	0.3456
1.00	0.2183	0.1893	0.2511	0.2565	0.2712	0.2862	0.2594	0.2680
1.05	0.2348	0.2147	0.2631	0.2656	0.2815	0.2934	0.2706	0.2763
1.10	0.2504	0.2336	0.2753	0.2766	0.2922	0.3027	0.2822	0.2870
1.15	0.2654	0.2513	0.2876	0.2883	0.3032	0.3124	0.2939	0.2980

Source: Author.

Figure 20 – Flow Distribution Charts - Round 2

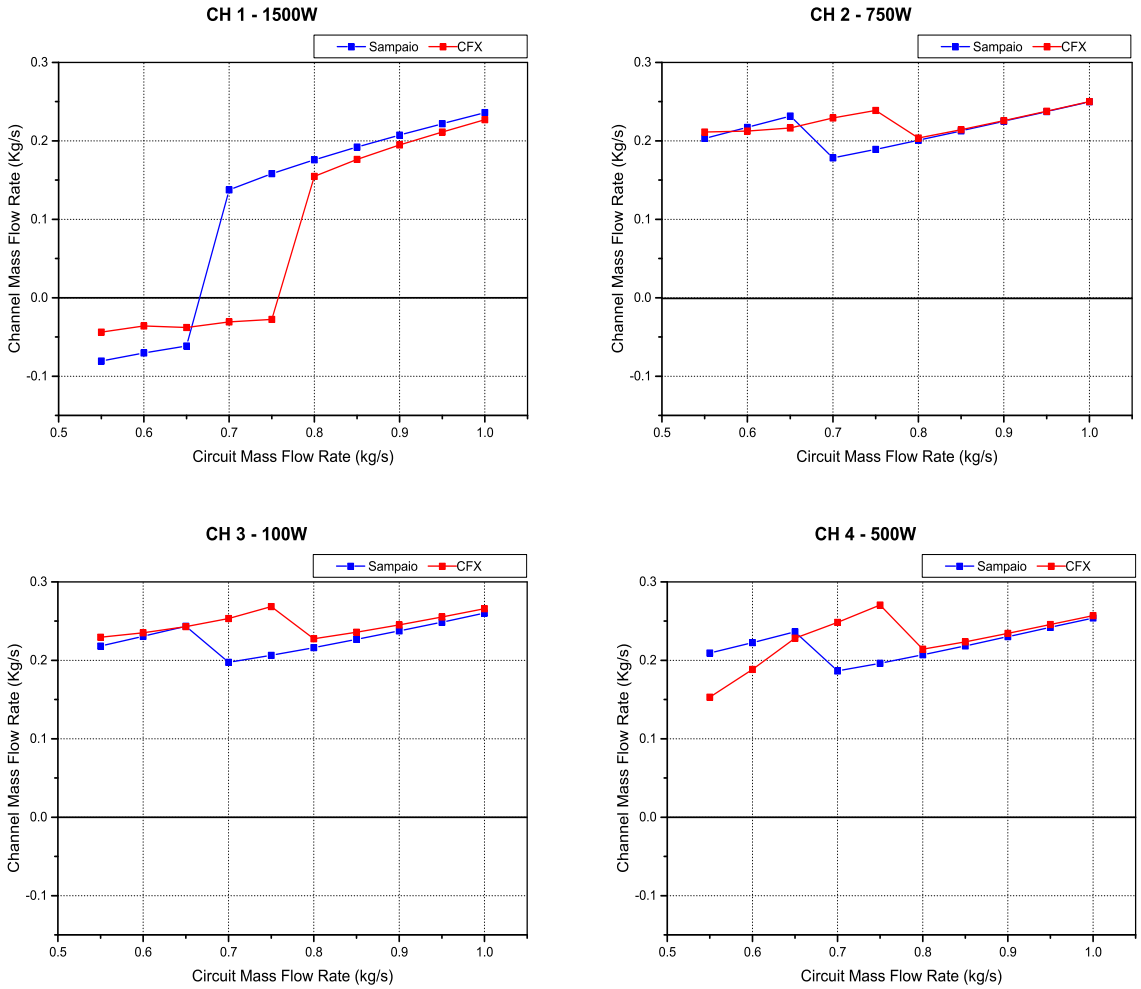

Source: Author.

Table 6 – 1D vs CFX 3D - Mass Flow Rate (Kg/s) results by Channel - Round 2

W_T	W_1		W_2		W_3		W_4	
	Sampaio	CFX	Sampaio	CFX	Sampaio	CFX	Sampaio	CFX
0.55	-0.0807	-0.0438	0.2031	0.2112	0.2183	0.2295	0.2094	0.1531
0.60	-0.0705	-0.036	0.2172	0.2126	0.2306	0.2350	0.2227	0.1884
0.65	-0.0615	-0.0379	0.2316	0.2165	0.2435	0.2429	0.2364	0.2283
0.70	0.1375	-0.0308	0.1784	0.2291	0.1976	0.2532	0.1865	0.2485
0.75	0.1583	-0.0277	0.1891	0.2388	0.2063	0.2685	0.1963	0.2705
0.80	0.1759	0.1547	0.2008	0.2036	0.2162	0.2275	0.2071	0.2142
0.85	0.1920	0.1763	0.2128	0.2142	0.2267	0.2358	0.2185	0.2236
0.90	0.2072	0.1947	0.2251	0.2257	0.2376	0.2452	0.2301	0.2344
0.95	0.2219	0.2114	0.2374	0.2378	0.2487	0.2552	0.2420	0.2457
1,00	0.2361	0.2271	0.2498	0.2500	0.2601	0.2658	0.2539	0.2571

Source: Author.

Figure 21 – Flow Distribution Charts - Round 3

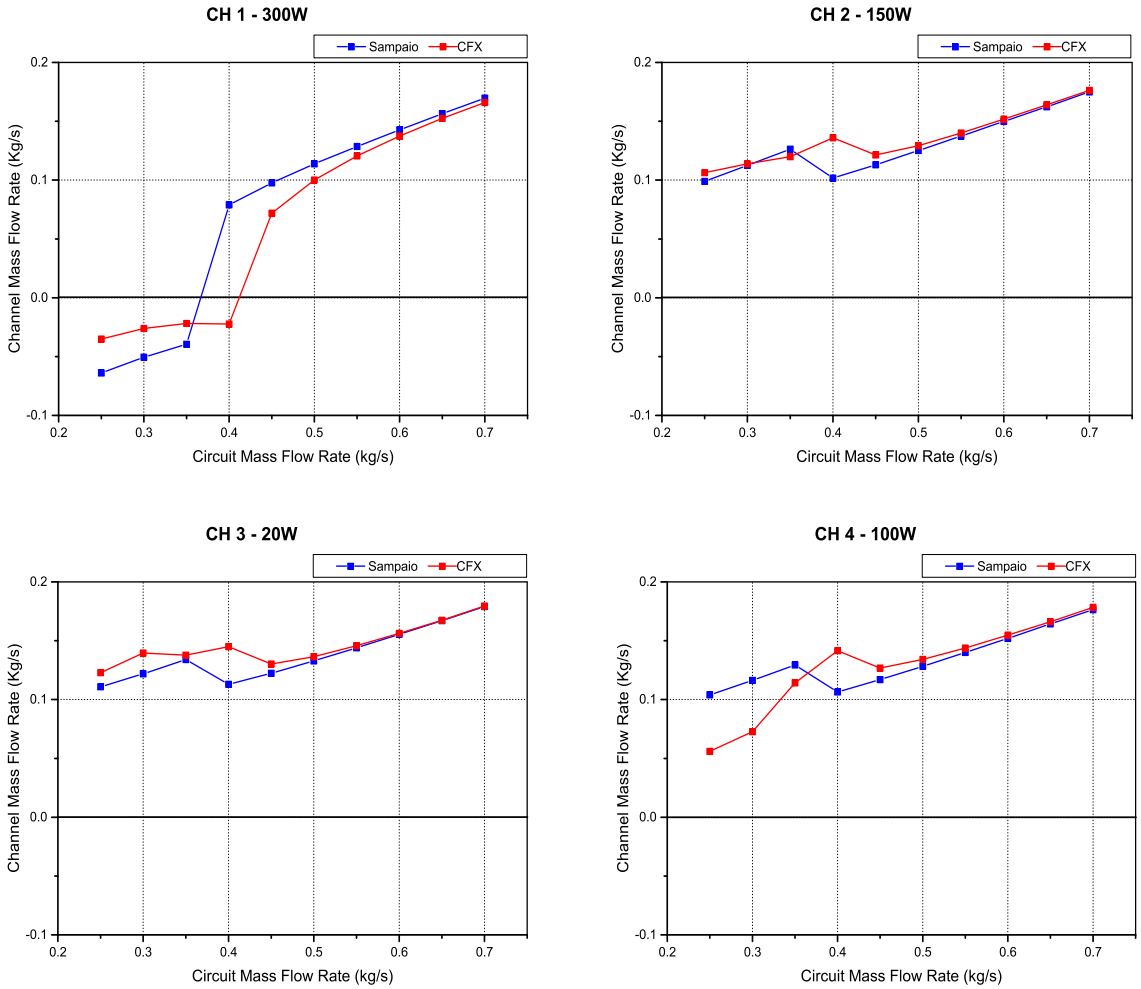

Source: Author.

Table 7 – 1D vs CFX 3D - Mass Flow Rate (Kg/s) results by Channel - Round 3

W_T	W_1		W_2		W_3		W_4	
	Sampaio	CFX	Sampaio	CFX	Sampaio	CFX	Sampaio	CFX
0.25	-0.0639	-0.0351	0.099	0.1063	0.1108	0.1229	0.1041	0.0559
0.30	-0.0506	-0.0261	0.1124	0.1138	0.1218	0.1396	0.1163	0.0727
0.35	-0.0396	-0.0218	0.1263	0.1198	0.1339	0.1378	0.1294	0.1142
0.40	0.0789	-0.0224	0.1017	0.1360	0.1130	0.1449	0.1065	0.1415
0.45	0.0976	0.0718	0.1131	0.1213	0.1224	0.1302	0.1169	0.1267
0.50	0.1138	0.1000	0.1251	0.1293	0.1328	0.1365	0.1283	0.1342
0.55	0.1286	0.1205	0.1375	0.1400	0.1439	0.1457	0.1401	0.1438
0.60	0.1427	0.1374	0.1499	0.1518	0.1554	0.1562	0.1521	0.1547
0.65	0.1563	0.1525	0.1624	0.1640	0.1671	0.1674	0.1642	0.1661
0.70	0.1697	0.1660	0.1749	0.1763	0.1790	0.1795	0.1765	0.1783

Source: Author.

In the results of the downward flow through four channels study, it can be seen a strong agreement between 3D CFX simulations and 1D Sampaio's model prediction.

In the first round result it can be seen a strong agreement between 3D CFX Simulations and 1D Sampaio's model prediction concerning mass flow rate distribution when a downward flow is established, i.e, prior to the flow reversion occurrence in the hot channel (CH1). However, it can also be noted that CFX simulations tended to onset a reversion pattern earlier, with a mass flow rate of 1.5 kg/s higher (roughly 15%) than Sampaio's model. Moreover, in the subsequent rounds (2 and 3), it seems to be a batter agreement in that regard when a lower heating power combination among the channels, as well as a lower total mass flow rate, is applied to the system, as can be seen in Fig. 22 that shows a comparison of CH1 reversion point results for each round. That behavior suggests that the way Sampaio's model treats the fluid properties over the radial channel direction in his model (with average values) can be a limiting factor in its capacity to well predict the reversion point in the hot channels. Those constant properties values assumption can make his model less sensitive to high heat flux conditions once that average values stand for a wide range of temperature at the near-wall flow domain. Furthermore, as that heat flux condition and its associated temperature gradient get lower, the average values tend to be more representative once it represents a shorter range of temperature, and the reversion point deviation tends to get smaller. That phenomenon can be observed in Fig. 23 where it is shown temperature flow curve over the radial hot channel direction 0.1m away from its entrance, for the first and third rounds.

Figure 22 – Channel 1 Reversion Point Comparison for Each Round.

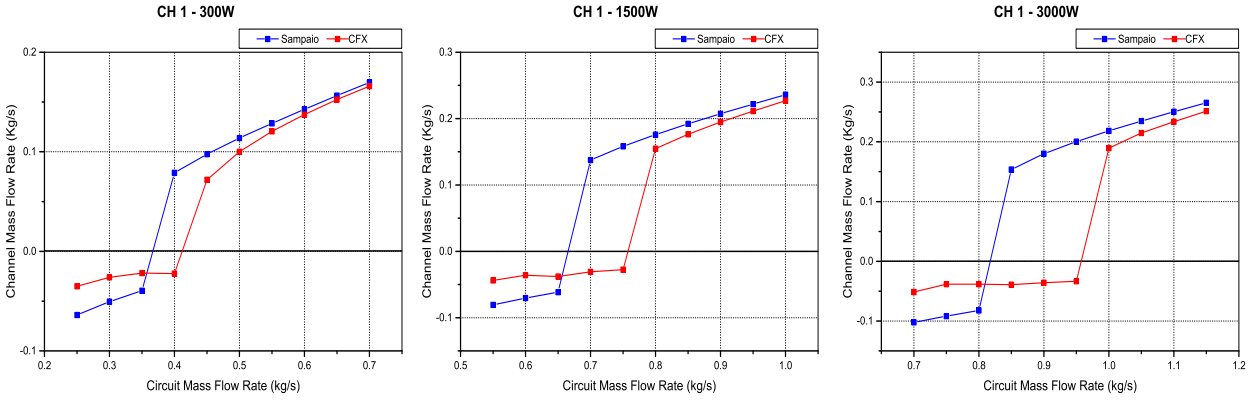

Source: Author.

Figure 23 – Schematic Arrange of the Flow Cross-Section (Round 1)

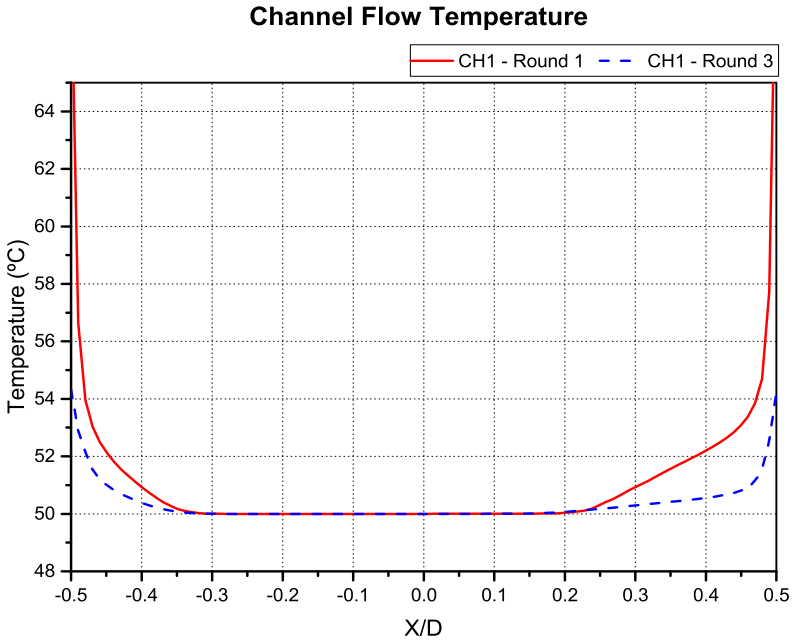

Source: Author.

6 Conclusions

Flow stability results of Sampaio's 1D model for a downward flow through two channels undergoing different heating powers were analyzed against 3D CFX simulation. It was shown that Sampaio's model results had a good agreement with CFX regarding the flow inversion.

Plenum geometry and size, as well as, channels heat flux profile influences on CFX simulations were analyzed. The results for both cases have shown those parameter having no significant influence on the flow inversion point.

Results for flow stability and distribution of Sampaio's model for a downward flow through four channel were analyzed against 3D CFX simulations. It was shown that Sampaio's model results had a good agreement with CFX modeling regarding flow distribution. Nevertheless, it was noted that for high heat flux values configurations, the total mass flow rate reversion point results in the hot channel tends to show some discrepancy. That behavior suggests there is some limitation in Sampaio's model on well reproducing near-wall effects due to its use of averaged fluid properties on the channel radial direction. Moreover, in that regard, it can be concluded that CFX 3D model tends to anticipate a flow reversion in comparison with Sampaio's model, whatever it is the flow condition.

Despite the reversion point divergence, results have shown that Sampaio's model could provide a good, fast and low-cost estimation of a potential unsafe operational condition of a pool-reactor.

Future works suggestions on Sampaio's model Using CFX simulation comprises:

- Flow stability and distribution analysis for several combinations of heating powers.
- Flow stability and distribution analysis for multiple channels.
- Flow stability and distribution analysis for open channels.
- Limitations analysis regarding near-wall effects of high heat flux on flow reversion.

Bibliography

AJIJUL, M.; MALEK, S.; SALAM, M.; KHANOM, S.; FAHAD, S. Assessment of n-16 activity concentration in bangladesh atomic energy commission triga research reactor. Nuclear Engineering and Technology, v. 50, p. 165–169, 2018.

ANSYS-INC. *CFX-Solver Theory Guide*. 2016. Disponível em: <https://www.sharcnet.ca/Software/Ansys/17.0/en-us/help/cfx_thry/i1299421.html#cfxBasiTranCont>. Acesso em: 03 Jul. 2019.

ANSYS-INC. *CFX-Solver Theory Guide*. 2016. Disponível em: <https://www.sharcnet.ca/Software/Ansys/17.0/en-us/help/cfx_thry/i1299782.html>. Acesso em: 03 Jul. 2019.

ANSYS-INC. *CFX-Solver Theory Guide*. 2016. Disponível em: <%https://www.sharcnet.ca/Software/Ansys/17.0/en-us/help/cfx_thry/i1302147.html>. Acesso em: 03 Jul. 2019.

ANSYS-INC. *CFX-Solver Theory Guide*. 2016. Disponível em: <https://www.sharcnet.ca/Software/Ansys/17.0/en-us/help/cfx_thry/cfxTurbTurbStat.html>. Acesso em: 03 Jul. 2019.

ANSYS-INC. *CFX-Solver Theory Guide*. 2016. Disponível em: <https://www.sharcnet.ca/Software/Ansys/17.0/en-us/help/cfx_thry/i1302321.html>. Acesso em: 03 Jul. 2019.

BAU, H.; TORRANCE, K. On the stability and flow reversal of an asymmetrically heated open convection loop. J. Fluid Mech., v. 106, p. 417–433, 1981.

BOURE, J. Sur un phénoméne de renversement du courant de réfrigération dans les canaux chauds d'une pile piscine refroidie in convection forcée. Repport CEA, n. l887, 1961.

BOURE, J. Review of two-phase flow instability. Nuclear Engineering and Design, n. 25, p. 165–192, 1973.

DURST, F.; RAY, S.; UNSAL, B.; BAYOUMI, O. The development lengths of laminar pipe and channel flows. *Journal of Fluids Engineering*, ASME, v. 127, p. 1154–1160, 2005.

FOX, R.; MCDONALD, A.; PRITCHARD, P. *Introdução à Mecânica dos Fluidos*. 6th. ed. Rio de Janeiro: LTC, 2006.

FUKUDA, K.; KATO, A.; HASEGAWA, S. Two-phase flow instability at low flow rate conditions. Journal Journal of Nuclear Science and Technology, v. 21, p. 491–500, 1984.

KIM, M.; YU, S.; KIM, H. Analyses on fluid flow and heat transfer inside calandria vessel of CANDU-6 using cfd. Nuclear Engineering and Design, v. 236, p. 1155–1164, 2006.

LEE, S.; VEZIROGLU, T.; KAKAC, S. Sustained and transient boiling flow instabilities in two parallel channel systems. Hemisphere Publishing Corp, p. 467–510, 1977.

PANDEY, V.; SINGH, S. Characterization of stability limits of Ledinegg instability and density wave oscillations for two-phase flow in natural circulation loops. Chemical Engineering Science, v. 168, p. 204–224, 2017.

PARK, J.; PARK, S.; JO, D.; CHAE, H.; LEE, B. Numerical analysis on flow inversion in a uniformly heated thin rectangular channel array. ICONE, 2014.

RAHARDJO, H.; WARDHANI, V. S. Effects of cooling fluid flow rate on the critical heat flux and flow stability in the plate fuel type 2 MW triga reactor. *Atom Indonesia*, v. 43, n. 3, p. 149–155, 2017.

REBROV, E.; SCHOUTEN, J.; CROON, M. Single-phase fluid flow distribution and heat transfer in microstructured reactors. Chemical Engineering Science, v. 66, p. 1374–1393, 2011.

SALIM, S.; CHEAH, S. Wall y+ strategy for dealing with wall-bounded turbulent flows. International Multi-Conference of Engineers and Computer Scientists, v. 2, 2009.

SAMPAIO, P. d. *Análise de Estabilidade para Escoamento Descendente em Canais Aquecidos*. Dissertação (Mestrado em Ciências e Engenharia Nuclear) — COPPE/UFRJ, Rio de Janeiro, September 1985.

SHAH, Y. *Thermal Energy: Sources, Recovery and Applications*. [S.l.]: CRC Press, 2018. v. 1.

SHARABI, M.; AMBRISINI, W.; HE, S. Prediction of unstable behaviour in a heated channel with water at supercritical pressure by CFD models. Annals of Nuclear Energy, v. 35, p. 767–782, 2008.

SMITH, R.; WOODRUFF, W. Thermal-hydraulic aspects of flow inversion in a research reactor, United States, 1986.

ANNEX A – DownFlow Program (Sampaio's Unidimensional Program)

```
! Modules
module nrtype
! assigning symbolic names ...
integer, parameter:: i4b=selected_int_kind(9)
integer, parameter:: i2b=selected_int_kind(4)
integer, parameter:: sp=kind(1.0)
integer, parameter:: dp=kind(1.0d0)
integer, parameter:: lgt=kind(.true.)
!
end module nrtype
module all_main_data
! Data associated to the CG solver
use nrtype
integer(i4b), parameter:: nmax=100 ! max. number of channels
integer(i4b):: nchannels ! actual number of channels
real(dp):: de(100) ! equivalent diameters (for 100 channels)
real(dp):: area(100) ! flow area (for 100 channels)
real(dp):: wnew(100) ! mass flow (for 100 channels)
real(dp):: wold(100) ! mass flow (for 100 channels)
real(dp):: W_total ! total mass flow
real(dp):: T_upper ! upper plenum temperature
real(dp):: T_lower ! lower plenum temperature
real(dp):: slength  ! length of the channels
real(dp):: toler   ! tolerance for convergence
real(dp):: Q(100) ! heating (for 100 channels)
real(dp):: Q_total ! Total hrating
real(dp):: deltap(100)
real(dp):: dpdw(100)
```

```
real(dp):: gamma
real(dp):: cp,dens_e,volesp_e,beta_e,dens_s,volesp_s,beta_s,visc_e,visc_s
real(dp):: bb(100),cc(100),ee(100),ff(100),gg(100),zz(100)
!
end module all_main_data
module fnames
! File names
character(80):: name7,name9,project,directory
!
end module fnames

program downflow
implicit none
call openfiles
call data_input
call initialise
call solver
call write_output
stop
end program downflow

subroutine openfiles
!-----------------------------------------------------
use nrtype
use fnames

implicit none
!-----------------------------------------------------

! The first file (unit 10) keeps the name of the directory of the input and output

open(unit=10,file='downflow.dat',status='old',form='formatted')
```

```
read(10,'(a)') project
read(10,'(a)') directory
close(10)

! Input file

name7=trim(directory)//trim(project)//'.dat'
write(*,'(a)') name7

name9=trim(directory)//trim(project)//'.out'
write(*,'(a)') name9

open(unit=7,file=name7,status='old',form='formatted')  ! Input data
open(unit=9,file=name9,status='unknown',form='formatted')  ! Output data

return
end subroutine openfiles

subroutine data_input

use nrtype
use all_main_data

implicit none

character(80):: dummy
character(27):: dummy27
integer(i4b):: i,j
!real(dp)::

! Read the input data file
```

```
read(7,'(a)') dummy
write(9,'(a)') dummy

read(7,'(a)') dummy
write(9,'(a)') dummy

read(7,'(a27,1x,i12)') dummy27,nchannels
write(9,'(a27,1x,i12)') dummy27,nchannels

read(7,'(a27,1x,f12.5)') dummy27,slength
write(9,'(a27,1x,f12.5)') dummy27,slength

read(7,'(a27,1x,f12.5)') dummy27,T_upper
write(9,'(a27,1x,f12.5)') dummy27,T_upper

read(7,'(a27,1x,f12.5)') dummy27,W_total
write(9,'(a27,1x,f12.5)') dummy27,W_total

read(7,'(a27,1x,f12.5)') dummy27,toler
write(9,'(a27,1x,f12.5)') dummy27,toler

read(7,'(a)') dummy
write(9,'(a)') dummy

read(7,'(a)') dummy
write(9,'(a)') dummy

read(7,'(a)') dummy
write(9,'(a)') dummy

do i=1,nchannels
read(7,'(i10,3(9x,d12.5))') j, de(j),area(j),Q(j)
```

```
write(9,'(i10,3(9x,d12.5))') j, de(j),area(j),Q(j)
end do

return
end subroutine data_input

subroutine initialise

use nrtype
use all_main_data

implicit none
integer(i4b):: i

cp=4180d0   ! specific heat at constant pressure

Q_total=0d0
do i=1,nchannels
Q_total=Q_total+Q(i)
wold(i)=W_total/nchannels
wnew(i)=wold(i)
end do

T_lower = T_upper + Q_total/(cp*W_total)

! Set properties

call water_properties(T_upper,dens_e,volesp_e,beta_e,visc_e)  ! properties at the u

call water_properties(T_lower,dens_s,volesp_s,beta_s,visc_s)  ! properties at the l

return
```

```
end subroutine initialise

subroutine solver

use nrtype
use all_main_data

implicit none
integer(i4b):: i,n,iconv,niter_max,iter
real(dp):: sum,resid

n=nchannels
gg(1)=1d0
ff(n)=W_total
niter_max=9999999
iconv=0

do iter=1,niter_max

call channels

do i=1,n
bb(i)=deltap(i)
cc(i)=dpdw(i)
end do

do i=1,n-1
ee(i)= -cc(i+1)/cc(i)
gg(i+1)=1d0-gg(i)*ee(i)
ff(i)=bb(i+1)-bb(i)+wold(i)*cc(i)-wold(i+1)*cc(i+1)
end do
```

```
sum=0d0
do i=1,n-1
zz(i)=ff(i)/cc(i)
sum=sum-gg(i)*zz(i)
end do

wnew(n)=(ff(n)+sum)/gg(n)

do i=n-1,1,-1
wnew(i)=zz(i)-ee(i)*wnew(i+1)      ! new guess
end do

!  Check convergence

resid=0d0
do i=1,n
resid=resid+dabs(wnew(i)-wold(i))/dabs(wold(i))
end do

if(resid.le.toler) then
iconv=1
exit
else
do i=1,n
wold(i)=wnew(i)
end do
end if

end do

sum=0d0
do i=1,n
```

```
sum=sum+1d0/dpdw(i)
end do
gamma=1d0/sum

if(iconv.eq.0) then
print*,'Does not converge after this number of iterations:', niter_max
else
print*,'Converged in this number of iterations:',iter
end if

return
end subroutine solver

subroutine water_properties(temp,dens,volesp,beta,visc)

use nrtype
use all_main_data

implicit none
real(dp), intent(in):: temp
real(dp), intent(out):: dens,volesp,beta,visc

real(dp):: a0,a1,a2,a3,a4,a5,b,t,t1,t2,t3,t4,t5,f,g,dfdt,dgdt,drhodt,c,bbb,xisc

a0=+999.83952d0
a1=+16.945176
a2=-7.9870401d-3
a3=-46.170461d-6
a4=+105.56302d-9
a5=-280.54253d-12
b=+16.879850d-3
```

```
t=temp
t2=t*t
t3=t2*t
t4=t2*t2
t5=t4*t

f=a0+a1*t+a2*t2+a3*t3+a4*t4+a5*t5
g=1d0+b*t
dens= f/g            ! density
volesp = 1d0/dens    !  specific volume

dfdt=a1+2d0*a2*t+3d0*a3*t2+4d0*a4*t3+5d0*a5*t4
dgdt=b

drhodt = dfdt/g - f*dgdt/(g*g)
beta=-drhodt/dens    ! volumetric thermal expansion coefficient

! computing viscosity...

c=7.47d-3
bbb=6.515d0
xisc=c*(temp-20d0)*(temp-20d0)-bbb*(temp-20d0)
xisc=xisc/(temp+273d0)
visc=1.001d-3*dexp(xisc)   ! viscosity

return
end subroutine water_properties

subroutine friction_factor(w_channel,visc,de_channel,area_channel,friction)

use nrtype
```

```
implicit none
real(dp), intent(in):: w_channel,visc,de_channel,area_channel
real(dp), intent(out):: friction
real(dp):: rey

rey=dabs(w_channel)*de_channel/(visc*area_channel)

if(rey.lt.2000d0) then
friction=64d0/rey
else if(rey.lt.4000d0) then
friction=0.032d0+4.396d-6*(rey-2000d0)
else
friction=0.0056d0+0.5d0*rey**(-0.32d0)
end if

return
end subroutine friction_factor

subroutine channels

use nrtype
use all_main_data

implicit none
integer(i4b):: i
real(dp):: cke,cks,w,de_channel,area_channel,Q_channel,friction
real(dp):: grav,c1,c2,c3,c4

cke=0.5d0
cks=1d0
grav=9.81d0
```

```
do i=1,nchannels

w=wold(i)
de_channel=de(i)
area_channel=area(i)
Q_channel=Q(i)

if(w.gt.0d0) then        ! downflow case

call friction_factor(w,visc_e,de_channel,area_channel,friction)

c1=0.5d0*volesp_e*( cke + cks + friction*slength/de_channel )/(area_channel*area_ch
c2=beta_e*Q_channel*volesp_e*(1d0+0.5d0*cks+0.25d0*friction*slength/de_channel)/(cp
c3=0.5d0*beta_e*Q_channel*dens_e*grav*slength/cp
c4=dens_e*grav*slength

deltap(i) = c1*w*w + c2*w + c3/w - c4

dpdw(i)  = 2d0*c1*w + c2  - c3/(w*w)

else                     ! upflow case

call friction_factor(w,visc_s,de_channel,area_channel,friction)

c1=0.5d0*volesp_s*( cke + cks + friction*slength/de_channel )/(area_channel*area_ch
c2=beta_s*Q_channel*volesp_s*(1d0+0.5d0*cks+0.25d0*friction*slength/de_channel)/(cp
c3=0.5d0*beta_s*Q_channel*dens_s*grav*slength/cp
c4=dens_s*grav*slength

deltap(i) = - c1*w*w + c2*w - c3/w - c4
dpdw(i)  = - 2d0*c1*w + c2  + c3/(w*w)
end if
```

```
end do

return
end subroutine channels

subroutine write_output

use nrtype
use all_main_data

implicit none
integer(i4b):: i

character(80):: heading1,heading2,heading3
character(6):: heading4
heading1='************************************'
heading2='Flow Distribution Results'
heading3='Channel No.          Flow Rate              DP(i)              DP(i)/DW(i)
heading4='Gamma='

write(9,'(a)') heading1
write(9,'(a)') heading2
write(9,'(a)') heading3

do i=1,nchannels
write(9,'(i10,3(9x,d12.5))') i, wnew(i), deltap(i), dpdw(i)
end do
write(9,'(a)') heading1
write(9,'(a6,1x,d12.5)') heading4,gamma

return
end subroutine write_output
```